Investigation on structures, luminescent and magnetic properties of Ln(III)–M (M = Fe–HS(II), Co–II) coordination polymers

ARTICLE *in* DALTON TRANSACTIONS · JANUARY 2011

Impact Factor: 4.2 · DOI: 10.1039/c0dt00516a · Source: PubMed

Dalton Transactions

Dynamic Article Links

Cite this: *Dalton Trans.*, 2011, **40**, 805

www.rsc.org/dalton

PAPER

Investigation on structures, luminescent and magnetic properties of Ln^{III}–M (M = Fe^{II}_{HS}, Co^{II}) coordination polymers†

Xiao-Qing Zhao, Ping Cui, Bin Zhao,* Wei Shi and Peng Cheng*

Received 21st May 2010, Accepted 18th October 2010
DOI: 10.1039/c0dt00516a

The structures, luminescent and magnetic properties of three series of coordination polymers with formulas-$\{[Fe_3Ln_2(L^1)_6(H_2O)_6]\cdot xH_2O\}_n$ (Ln = Pr-Er; **1–9**), $\{[Co_3Ln_2(L^1)_6(H_2O)_6]\cdot yH_2O\}_n$ (Ln = Pr-Dy, Yb; **10–17**) and $\{[Co_2Ln(L^2)(HL^2)_2(H_2O)_7]\cdot zH_2O\}_n$ (Ln = Eu-Yb; **18–25**) (H_2L^1 = pyridine-2,6-dicarboxylic acid, H_3L^2 = 4-hydroxyl-pyridine-2,6-dicarboxylic acid) were systematically explored in this contribution. [Fe^{II}_{HS}–L^1–Ln^{III}] (**1–9**) and [Co^{II}–L^1–Ln^{III}] (**10–17**) series are isostructural, and display 3D porous networks with 1D nanosized channels constructed by Fe/Co-OCO-Ln linkages. Furthermore, two types of "water" pipes are observed in 1D channels. [Co^{II}–L^2–Ln^{III}] (**18–25**) series exhibit 2D open frameworks based on double-stranded helical motifs, which are further assembled into 3D porous structures by intermolecular hydrogen bonds between hydroxyl groups. The variety of the resulting structures is mainly due to the HO-substitution effect. These 3D coordination polymers show considerably high thermal stability, and do not decomposed until 400 °C. The high-spin Fe^{II} ion in [Fe^{II}_{HS}–L^1–Ln^{III}] was confirmed by X-ray photoelectron spectroscopy, Mössbauer spectroscopy and magnetic studies. The luminescent spectra of coordination polymers associated with Sm^{III}, Eu^{III}, Tb^{III} and Dy^{III} were systematically investigated, and indicate that different *d*-metal ions in *d*-*f* systems may result in dissimilar luminescent properties. The magnetic properties of [Fe^{II}_{HS}–L^1–Ln^{III}] (**3**, **6**, **7**, **9**, **13**), [Co^{II}–L^1–Ln^{III}] (**15–17**) and [Co^{II}–L^2–Ln^{III}] (**19–24**) coordination polymers were also studied, and the $\chi_M T$ values decrease with cooling. For the single ion behavior of Co^{II} and Ln^{III} ions, the magnetic coupling nature between Fe^{II}_{HS}/Co^{II} and Ln^{III} ions cannot be clearly depicted as antiferromagnetic coupling.

Introduction

In the last few decades, with the rapid development of coordination polymers, the selective introduction of *d*- and *f*-block metal ions into the same supramolecular entity has led to a wide variety of heteronuclear coordination polymers and has attracted special attention, due to their diversified and tunable frameworks or electronic structures[1] and versatile applications as functional materials in magnetism,[2] luminescence,[3] adsorption,[4] catalysis[5] and others.[6] Among all the heteronuclear edifices, the majority are associated with Cu–Ln systems,[7–9] which contain one-dimensional chains and ladders,[7] two-dimensional grids[8] and three-dimensional porous networks and interpenetrated modes,[9] while a few with Mn–Ln,[10] Ni–Ln,[11] Cr–Ln,[12] Fe–Ln,[13,14] Co–Ln,[15,16] Zn–Ln[16d,17] and some 4*d*-4*f*[18] or 5*d*-4*f*[19] systems are reported. In the reported literature on Fe/Co–Ln, $[Fe(CN)_6]^{3-/4-}$ and $[Co(CN)_6]^{3-/4-}$ are always used as building blocks to construct infinite polymeric arrays supported by cyanide bridges,[13,15] and those bridged directly by organic ligands are rarely limited. Fe^{II} is easily oxidized to Fe^{III} under normal conditions, especially in water solution. If Fe^{II} need to be incorporated into the framework of a coordination polymer, normally, the reaction should be progressed without oxygen. Furthermore, Fe^{II} (d^6) displays two different electronic configurations in pseudo-octahedral surroundings: diamagnetic low-spin state ($^1A_1$) and paramagnetic high-spin state ($^5T_2$).[20] With the competitive reaction between Fe^{II} and Ln^{III} with organic linkers, it is extremely arduous to construct heteronuclear coordination polymers containing both Fe^{II} and Ln^{III}. As far as we know, the literature reporting several discrete dimetallic examples comprising high-spin Fe^{II} and Ln^{III} ions, is rare.[14b–d] Co^{II} (d^7) is the neighbor of Fe^{II}, and comparatively stable in contrast to Fe^{II}. Usually, Co^{II} ion possesses a first-order orbital momentum with magnetic anisotropy when it is in pseudo-octahedral surroundings, and it has been researched in complexes for a long time for its unique magnetic property. When combining Co^{II} and Ln^{III} ions into one system, the resultant system may exhibit unique magnetic properties differing from that of the homometallic system, but for

Department of Chemistry, Nankai University, Tianjin, 300071, People's Republic of China. E-mail: zhaobin@nankai.edu.cn, pcheng@nankai.edu.cn

† Electronic supplementary information (ESI) available: Explanation to the alert level A in CheckCIF; some figures including PXRD, TGA, XPS, luminescence (Figure S2–S7). CCDC reference numbers 630836, 630837, 630839, 630840 and 772801–772815. For ESI and crystallographic data in CIF or other electronic format see DOI: 10.1039/c0dt00516a

both their orbital contribution/single ion behaviour, the magnetic interactions are always extremely difficult to interpret. Thus, Co–Ln systems are an interesting but less developed field for chemical researchers.

As reviewed by Shore and coworkers,[21] the [M-linkers-Ln] system is one type of existing *d-f* coordination polymer. The class of [M–CN–Ln] is the pioneer traced back to 1916,[22] and [M–CO–Ln] is another group developed later in the 1970s.[23] Subsequently, carboxylic acids, amino acids, bipyridyl, and other multidentate ligands were used to bridge *d*- and *f*-metal ions.[24] Among them, pyridine carboxylic acids have been found to be good linkers between *d*- and *f*-metal ions.[25] There are three interesting characteristics of this kind of ligands: i) the carboxyl groups provide rich binding coordination modes to connect different metal ions; ii) the rigid pyridine rings can assist in the generation of non-interpenetrated structures; iii) since the carboxyl groups can rotate in a limited way, they may link metal ions in different directions, resulting in various fascinating topologies. For example, Hong and coworkers made some strides toward the *d-f* coordination polymers based on pyridine carboxylic acids (such as pyridine-2,5-dicarboxylic acid, pyridine-2,4-dicarboxylic acid),[7b,24b,26] and Yang and coworkers construct multinuclear Cu–Ln coordination polymers employing the rigid isonicotinic acid as ligand.[27] Our group also made some contributions on the assembly of pyridine dicarboxylic acid, *d*- and *f*-metal ions.[10d–g,17c]

Considering the above lines and inspired by our previous work, we chose Fe^{II} as *d*-metal ions to built *d-f* heterometallic coordination polymers, and excitingly, high-spin Fe^{II} was successfully introduced into *d-f* systems under harsh hydrothermal conditions, resulting in nine 3D porous [Fe^{II}_{HS}–L^1–Ln^{III}] coordination polymers with formula-$\{[Fe_3Ln_2(L^1)_6(H_2O)_6]\cdot xH_2O\}_n$ (Ln = Pr-Er; **1–9**) (L^1 = pyridine-2,6-dicarboxylate anions). If the high-spin Fe^{II} is replaced by Co^{II}, what would happen in the structure? As a result, a series of [Co^{II}–L^1–Ln^{III}] coordination polymers -$\{[Co_3Ln_2(L^1)_6(H_2O)_6]\cdot yH_2O\}_n$ (Ln = Pr-Dy, Yb; **10–17**) were obtained, which is isomorphous to the series of [Fe^{II}_{HS}–L^1–Ln^{III}]. Furthermore, we wanted to investigate whether the HO-substituted ligand would affect the structure, and then we chose 4-hydroxyl-pyridine-2,6-dicarboxylic acid (H_3L^2) instead of H_2L^1 as ligand to synthesize Co–Ln complexes, resulting in a series of 2D coordination polymers-$\{[Co_2Ln(L^2)(HL^2)_2(H_2O)_7]\cdot zH_2O\}_n$ (Ln = Eu-Yb; **18–25**) based on double-stranded helical motifs. **4–6**, **11** and **14** appearing in this paper have already been published elsewhere as communications.[28] We now present these coordination polymers as a part of our work to systematically compare and investigate the structures and properties of three series of coordination polymers, and expect to provide some insight into further construction of *d-f* coordination polymers with novel luminescent and magnetic or other potential properties.

Experimental section

Materials and physical techniques

All reagents and solvents employed were commercially available and used as received without further purification. Elemental analyses for C, H and N were carried out by using a Perkin–Elmer analyzer. Thermal analyses (under oxygenated atmosphere, heating rate of 10 °C min^{-1}) were carried out in a Labsys NETZSCH TG 209 Setaram apparatus. XPS spectra were recorded using a Kratos Axis Ultra DLD multi-technique X-ray photoelectron spectroscopy employing a monochromated Al-Ka X-ray source. The Mössbauer spectra were measured by an Oxford MS-500 model constant acceleration Mössbauer spectrometer with a 1024 multichannel analyzer. The velocity was calibrated by an α-Fe foil. The radiation source was 57Co/Rh. A xenon (methane) proportional counter was used as a detector. Computer fits were performed to all measured data. The fluorescent spectra of **3**, **4**, **6** and **7** were measured on a WFY-10 spectrometer and those of **12**, **13**, **15** and **16** on a Varian Cary Eclipse Fluorescence spectrophotometer. Variable-temperature magnetic susceptibilities were measured on a Quantum Design MPMS-7 SQUID magnetometer. Diamagnetic corrections were applied with Pascal's constants for all the constituent atoms.

Syntheses of $\{[Fe_3Ln_2(L^1)_6(H_2O)_6]\cdot xH_2O\}_n$ (Ln = Pr, x = 7, (1); Ln = Nd, x = 7, (2); Ln = Sm, x = 7, (3); Ln = Dy, x = 8, (7); Ln = Ho, x = 7, (8); Ln = Er, x = 7, (9))

A mixture of H_2L^1 (1.2 mmol, 0.200 g), $FeSO_4\cdot 7H_2O$ (0.6 mmol, 0.167 g), lanthanide oxide (Pr_4O_7, Nd_2O_3, Sm_2O_3, Dy_2O_3, Ho_2O_3) (0.1 mmol) or hydroxide ($Er(OH)_3$) (0.2 mmol), CH_3CN (4 mL) and H_2O (8 mL) was placed in a 25 mL Teflon-lined steel vessel and heated to 180 °C for 3 days, then cooled to room temperature at a rate of 1.5° h^{-1}. The resulting dark-red prism-shaped crystals were collected after washing with H_2O. The yields and elemental analyses are listed in Table 1 (except **2**, the elemental analyses of others are performed after vacuum drying).

Syntheses of $\{[Co_3Ln_2(L^1)_6(H_2O)_6]\cdot yH_2O\}_n$ (Ln = Pr, y = 7, (10); Ln = Sm, y = 7, (12); Ln = Eu, y = 7, (13); Ln = Tb, y = 6, (15); Ln = Dy, y = 7, (16); Ln = Yb, y = 6, (17))

A mixture of H_2L^1 (0.8 mmol, 0.134 g), CoO (0.6 mmol, 0.045 g), $Ln(NO_3)_3\cdot 6H_2O$ (0.2 mmol) and H_2O (8 mL) was placed in a 25 mL Teflon-lined steel vessel and heated to 180 °C for 3 days, then cooled to room temperature at a rate of 1.5° h^{-1}. The resulting red prism-shaped crystals were collected after washing with H_2O and diethyl ether. The yields and elemental analyses are listed in Table 1.

Syntheses of $\{[Co_2Ln(L^2)(HL^2)_2(H_2O)_7]\cdot zH_2O\}_n$ (Ln = Eu, z = 9, (18); Ln = Gd, z = 9, (19); Ln = Tb, z = 10, (20); Ln = Dy, z = 2, (21); Ln = Ho, z = 3, (22); Ln = Er, z = 4, (23); Ln = Tm, z = 9, (24); Ln = Yb, z = 9, (25))

A mixture of H_3L^2 (0.3 mmol, 0.055 g), $Co(OAc)_2\cdot 4H_2O$ (0.2 mmol, 0.049 g), $Ln(OH)_3$ (0.1 mmol) and H_2O (10 mL) was placed in a 25 mL Teflon-lined steel vessel and heated to 160 °C for 3 days, then cooled to room temperature at a rate of 1.5° h^{-1}. The resulting red block-shaped crystals were collected after washing with H_2O and diethyl ether. The yields and elemental analyses are listed in Table 1.

X-ray crystallographic study

Suitable single crystals were selected for single-crystal X-ray diffraction analysis. The intensity data of **1–3**, **8–10**, **12**, **13** and **15–17** were collected on a computer-controlled Bruker SMART 1000

Table 1 Yields and elemental analyses (calculated and experimental) for **1–3**, **7–10**, **12**, **13** and **15–25**

		Elemental analyses Calculated (%)			Elemental analyses Experimental (%)		
	Yield (%) based on Ln	C	H	N	C	H	N
1	20	30.13	2.65	5.02	30.60	2.81	4.92
2·H_2O	56	29.69	2.73	4.95	30.11	2.88	5.10
3	62	29.79	2.62	4.96	30.80	2.69	5.13
7	48	29.31	2.80	4.56	29.04	2.65	4.84
8	57	29.29	2.58	4.88	30.32	2.29	5.05
9	61	29.21	2.57	4.87	30.51	2.24	5.09
10·$2H_2O$	63	29.49	2.83	4.91	28.97	2.99	5.15
12·$2H_2O$	60	29.17	2.80	4.86	28.46	2.31	5.12
13·$2H_2O$	65	29.12	2.79	4.85	29.62	2.80	5.11
15·$3H_2O$	70	28.89	2.77	4.81	28.12	2.72	5.20
16·$2H_2O$	60	28.77	2.76	4.79	28.69	2.67	5.14
17·$3H_2O$	62	28.42	2.73	4.74	28.70	2.76	5.01
18	50	22.92	3.66	3.82	22.65	3.96	4.31
19	51	22.81	3.65	3.80	22.98	3.26	4.23
20	42	22.23	3.82	3.70	21.85	4.21	4.00
21	48	25.61	2.66	4.27	24.98	3.26	4.62
22	55	25.09	2.81	4.18	24.29	3.32	4.54
23	50	24.59	2.95	4.10	23.87	3.76	4.43
24	63	22.57	3.61	3.76	21.93	4.03	4.14
25	40	22.49	3.60	3.75	22.06	3.96	4.05

CCD diffractometer equipped with graphite-monochromated $Mo_{K\alpha}$ radiation (λ = 0.71073 Å), those of **18** were collected on an Oxford Diffractometer SuperNova TM, and those of **19–25** were collected on a Rigaku Saturn CCD diffractometer equipped with confocal-monochromated $Mo_{K\alpha}$ radiation (λ = 0.71070 Å). Adsorption corrections were performed using the multi-scan method. The structures were solved by the direct method and refined by the full-matrix least-squares method on F^2 with anisotropic thermal parameters for all non-hydrogen atoms.[29] The hydrogen atoms on the carbon atoms were placed in a calculated position with isotropic displacement parameters set to 1.2 U_{eq} of the attached atom, and those on hydroxyl group set to 1.5 U_{eq}(O). The hydrogen atoms on the coordinated water molecules were located in a difference Fourier map, and those of lattice water molecules were not included in those coordination polymers. Crystal data, data collection parameters, and refinement statistics for **1–3**, **8–10**, **12**, **13** and **15–25** are listed in Tables 2 and 3. CCDC numbers 772810 (**1**), 772808 (**2**), 772812 (**3**), 772807 (**8**), 772803 (**9**), 772809 (**10**), 772811 (**12**), 630836 (**13**), 630839 (**15**), 630837 (**16**), 630840 (**17**), 772804 (**18**), 772805 (**19**), 772813 (**20**), 772801 (**21**), 772806 (**22**), 772802 (**23**), 772814 (**24**) and 772815 (**25**) contain the supplementary crystallographic data for this paper.†

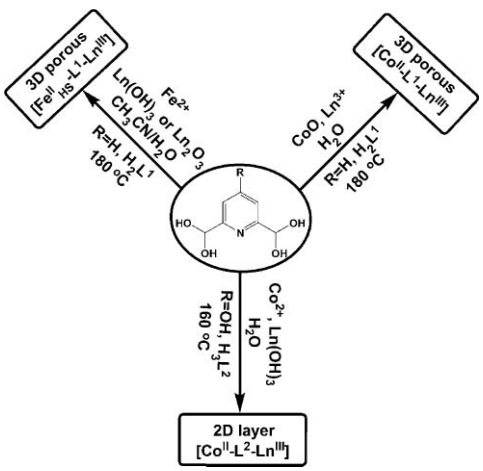

Scheme 1 Reaction scheme for the series of [Fe^{II}_{HS}–L^1–Ln^{III}], [Co^{II}–L^1–Ln^{III}] and [Co^{II}–L^2–Ln^{III}].

Results and discussion

The series of [Fe^{II}_{HS}–L^1–Ln^{III}] coordination polymers (**1–9**) were prepared according to the method reported previously,[28a] by the hydrothermal reaction of H_2L^1, $FeSO_4$·$7H_2O$ and lanthanide oxide or hydroxide in a mixture of CH_3CN and H_2O at 180 °C, the isomorphous [Co^{II}–L^1–Ln^{III}] coordination polymers (**10–17**) were obtained by mixing H_2L^1, CoO and $Ln(NO_3)_3$·$6H_2O$ in H_2O under hydrothermal conditions at 180 °C,[28b] and the series of [Co^{II}–L^2–Ln^{III}] coordination polymers (**18–25**) were produced by mixing H_3L^2, $Co(OAc)_2$·$4H_2O$, $Ln(OH)_3$ and H_2O under hydrothermal conditions at 160 °C, as shown in Scheme 1. The [Fe^{II}_{HS}–L^1–Ln^{III}] coordination polymers were synthesized in a mixture of CH_3CN and H_2O, and CH_3CN may play an important role in the survival of Fe^{II} ions under harsh hydrothermal conditions. In all the reactions, lanthanide oxide/hydroxide or cobalt oxide were used as base to neutralize acidic ligands, and then the deprotonated carboxylate groups were easy to bond to metal ions.

The structural determinations of **1–3**, **8–10**, **12**, **13** and **15–25** were performed by single-crystal X-ray diffraction analyses, and for **7** we did not collect the crystallographic data due to the small crystalline samples. The powder X-ray diffraction pattern displayed that **7** was isostructural to other [Fe^{II}_{HS}–L^1–Ln^{III}] analogues, and elemental and thermogravimetric analyses can determine the lattice water molecules, displaying eight uncoordinated water molecules per [Fe_3Dy_2] unit (see Supporting Information, ESI†).

Table 2 Crystallographic data for **1–3**, **8–10**, **12**, **13** and **15**

	1	**2**	**3**	**8**	**9**	**10**	**12**	**13**	**15**
Formula	$C_{42}H_{44}Fe_3N_6O_{37}Pr_2$	$C_{42}H_{44}Fe_3N_6Nd_2O_{37}$	$C_{42}H_{44}Fe_3N_6O_{37}Sm_2$	$C_{42}H_{44}Fe_3Ho_2N_3O_{37}$	$C_{42}H_{44}Er_2Fe_3N_6O_{37}$	$C_{42}H_{44}Co_3N_6O_{37}Pr_2$	$C_{42}H_{44}Co_3N_6O_{37}Sm_2$	$C_{42}H_{44}Co_3Eu_2N_6O_{37}$	$C_{42}H_{42}Co_3N_6O_{36}Tb_2$
M_r/g mol^{-1}	1674.20	1680.86	1693.08	1722.24	1726.90	1683.44	1702.32	1705.54	1701.45
T/K	293(2)	293(2)	293(2)	293(2)	293(2)	294(2)	294(2)	294(2)	294(2)
Crystal System	Hexagonal	Hexagonal	Hexagonal	Hexagonal	Hexagonal	Hexagonal	Hexagonal	Hexagonal	Hexagonal
Space group	*P6/mcc*	*P6/mcc*	*P6/mcc*	*P6/mcc*	*P6/mcc*	*P6/mcc*	*P6/mcc*	*P6/mcc*	*P6/mcc*
a/Å	15.514(2)	15.329(3)	15.4050(14)	15.187(2)	15.165(7)	15.4997(9)	15.3092(14)	15.2806(10)	15.288(4)
b/Å	15.514(2)	15.329(3)	15.4050(14)	15.187(2)	15.165(7)	15.4997(9)	15.3092(14)	15.2806(10)	15.288(4)
c/Å	15.354(4)	15.403(6)	15.456(3)	15.616(4)	15.713(8)	15.2348(17)	15.346(3)	15.393(2)	15.571(9)
α (°)	90	90	90	90	90	90	90	90	90
β (°)	90	90	90	90	90	90	90	90	90
γ (°)	120	120	120	120	120	120	120	120	120
V/Å^3	3200.4(11)	3134.5(15)	3176.5(7)	3119.2(10)	3129(3)	3169.7(4)	3114.8(7)	3112.7(5)	3152(2)
Z	2	2	2	2	2	2	2	2	2
ρ_{calcd}/g cm^{-3}	1.737	1.781	1.770	1.834	1.833	1.764	1.815	1.820	1.793
μ/mm^{-1}	2.256	2.406	2.588	3.289	3.432	2.376	2.739	2.870	3.086
F(000)	1660	1664	1672	1692	1696	1666	1678	1682	1670
θ (°)	2.65 to 26.28	2.66 to 26.19	1.53 to 26.22	2.68 to 26.41	2.59 to 26.38	2.67 to 26.35	2.66 to 26.41	3.76 to 26.34	2.66 to 26.27
Refl. collected/unique (R(int))	16438/1135 (0.1123)	15963/1095 (0.1127)	15956/1114 (0.0580)	16395/1113 (0.0599)	16725/1115 (0.0477)	16432/1134 (0.0473)	15942/1113 (0.0913)	15944/1103 (0.0669)	16034/1111 (0.0803)
GOF on F^2	1.102	1.138	0.916	1.147	1.008	1.134	1.080	1.096	1.071
R_1/wR_2 [$I>2\sigma(I)$]	0.0304/0.0901	0.0381/0.0832	0.0343/0.0850	0.0266/0.0608	0.0272/0.0831	0.0262/0.0725	0.0338/0.0790	0.0266/0.0678	0.0273/0.0658
R_1/wR_2 (all data)	0.0432/0.0995	0.0609/0.0919	0.0667/0.1121	0.0409/0.0683	0.0428/0.0904	0.0394/0.0804	0.0670/0.0981	0.0476/0.0780	0.0528/0.0781
Largest diff. peak/hole (e Å^{-3})	0.949/–0.610	1.491/–0.572	1.094/–1.012	0.475/–0.467	1.438/–1.066	0.914/–0.614	1.244/–1.167	0.861/–0.964	0.847/–1.050

Table 3 Crystallographic data for **16–25**

	16	**17**	**18**	**19**	**20**	**21**	**22**	**23**	**24**	**25**
Formula	$C_{42}H_{44}Co_3Dy_2N_6O_{37}$	$C_{42}H_{42}Co_3N_6O_{36}Yb_2$	$C_{21}H_{40}Co_2EuN_3O_{31}$	$C_{21}H_{40}Co_2GdN_3O_{31}$	$C_{21}H_{42}Co_2N_3O_{32}Tb$	$C_{21}H_{26}Co_2DyN_3O_{24}$	$C_{21}H_{28}Co_2HoN_3O_{25}$	$C_{21}H_{30}Co_2ErN_3O_{26}$	$C_{21}H_{40}Co_2N_3O_{31}Tm$	$C_{21}H_{40}Co_2N_3O_{31}Yb$
M_r/g mol^{-1}	1726.62	1729.69	1100.38	1105.67	1125.37	984.81	1005.25	1025.60	1117.35	1121.46
T/K	294(2)	293(2)	293(2)	113(2)	113(2)	293(2)	293(2)	293(2)	113(2)	113(2)
Crystal system	Hexagonal	Hexagonal	Monoclinic	Monoclinic	Monoclinic	Monoclinic	Monoclinic	Monoclinic	Monoclinic	Monoclinic
Space group	*P6/mcc*	*P6/mcc*	$P2_1/c$	$P2_1/c$	$P2_1/c$	$P2_1/c$	$P2_1/c$	$P2_1/c$	$P2_1/c$	$P2_1/c$
a/Å	15.2196(8)	15.0144(8)	8.9767(4)	8.8952(18)	8.8872(18)	8.939(5)	8.9629(18)	8.9328(18)	8.8971(18)	8.8997(18)
b/Å	15.2196(8)	15.0144(8)	23.9151(10)	24.379(5)	23.960(5)	24.460(14)	24.304(5)	24.341(5)	23.867(5)	23.845(5)
c/Å	15.4737(15)	15.6165(17)	18.6746(9)	18.159(5)	18.493(5)	18.213(9)	18.353(5)	18.192(5)	18.486(5)	18.414(5)
α (°)	90	90	90	90	90	90	90	90	90	90
β (°)	90	90	111.497(4)	109.94(3)	110.57(3)	110.34(2)	110.35(3)	110.27(3)	110.72(3)	110.70(3)
γ (°)	120	120	90	90	90	90	90	90	90	90
V/Å^3	3104.1(4)	3048.8(4)	3730.2(3)	3701.8(15)	3686.8(15)	3734(4)	3748.4(15)	3710.6(15)	3671.6(15)	3655.4(15)
Z	2	2	4	4	4	4	4	4	4	4
ρ_{calcd}/g cm^{-3}	1.847	1.884	1.959	1.982	2.027	1.752	1.781	1.836	2.021	2.038
μ/mm^{-1}	3.264	3.938	2.654	2.772	2.906	2.948	3.057	3.221	3.405	3.551
F(000)	1694	1690	2208	2212	2256	1940	1984	2028	2232	2236
θ [°]	3.09 to 26.38	1.57 to 26.34	2.44 to 25.10	2.05 to 25.10	2.07 to 25.01	2.39 to 25.01	2.37 to 25.01	2.39 to 25.01	1.71 to 25.01	2.08 to 25.01
Refl. collected/unique (R(int))	15971/1108 (0.0552)	15667/1090 (0.0497)	14276/6597 (0.0532)	27848/6518 (0.0636)	26901/6411 (0.0445)	27283/6525 (0.1868)	22751/6557 (0.0838)	22405/6487 (0.0645)	27158/6431 (0.0531)	27291/6393 (0.0489)
GOF on F^2	1.177	1.151	1.087	1.126	1.135	1.042	1.081	1.049	1.120	1.131
R_1/wR_2 [$I>2\sigma(I)$]	0.0235/0.0588	0.0241/0.0739	0.0772/0.1881	0.0670/0.1317	0.0910/0.1995	0.0797/0.1829	0.0649/0.1498	0.0455/0.1139	0.0481/0.1029	0.0493/0.0965
R_1/wR_2 (all data)	0.0410/0.0706	0.0397/0.0860	0.0988/0.1965	0.0728/0.1348	0.0944/0.2012	0.1081/0.2034	0.0890/0.1661	0.0546/0.1196	0.0498/0.1038	0.0512/0.0975
Largest diff. peak/hole (e Å^{-3})	0.505/–0.581	0.955/–0.409	3.984/–1.766	4.685/–2.374	4.983/–3.504	3.586/–2.045	1.603/–0.983	2.644/–1.445	1.823/–0801	1.797/–0.865

Structural description of [Fe^{II}_{HS}–L^1–Ln^{III}] and [Co^{II}–L^1–Ln^{III}] coordination polymers

Well-grown crystals of [Fe^{II}_{HS}–L^1–Ln^{III}] and [Co^{II}–L^1–Ln^{III}] coordination polymers suitable for single-crystal X-ray diffraction study are obtained by using hydrothermal synthesis, and the results show that two series of coordination polymers are isomorphous, which crystallize in the hexagonal system, *P6/mcc* space group. We chose polymer **1**-[Fe^{II}_{HS}–L^1–Pr^{III}] as a representative to depict this structure briefly, and compare the difference between these isostructural polymers. Fig. 1 shows the coordination environments of Fe^{II}_{HS}, Pr^{III} ions and the building units in **1**. Each Pr^{III} ion coordinates with three tridentate L^1, forming the building block-[$Pr(L^1)_3$], and Pr^{III} ion lies on the intersection of three- and two-fold axes. The remaining coordination sites in $Pr(L^1)_3$ coordinate to Fe^{II} ions and the bridging carboxyl groups adopt *syn-anti* bidentate mode. The coordination environment of Fe^{II}_{HS} ion consists of four carboxylate O atoms and two water molecules, forming another building block-[$FeO_4(H_2O)_2$], and Fe^{II}_{HS} ion lies on the intersection of a two-fold axis and a mirror plane. The overall framework can be viewed as the self-assembly of two different types of building blocks-[$Pr(L^1)_3$] and [$FeO_4(H_2O)_2$]. Each [$Pr(L^1)_3$] is surrounded by six [$FeO_4(H_2O)_2$] in its vicinity, while each [$FeO_4(H_2O)_2$] has four [$Pr(L^1)_3$] as the nearest neighbors, and the linkers are carboxyl groups. As a result of this connection, [$Pr(L^1)_3$] and [$FeO_4(H_2O)_2$] building blocks are arrayed alternately by carboxyl groups, forming the 3D porous framework similar to those of the reported [Mn^{II}–L^1–Ln^{III}],[10d–g] and the 1D channel extends along the *c* axis (Fig. 2a). The walls of the 1D channel are constructed by Fe^{II}_{HS} and Pr^{III} ions with Fe–OCO–Pr connection, and the distance between Fe^{II}_{HS} and Pr^{III} ions is 5.898 Å, while the diameter of the 1D channel is 17.91 Å (defined by the separation between two opposite Pr^{III} ions). Furthermore, the wall of the 1D channel can be viewed as an infinite interweaving left- and right-hand sextuple-stranded helix with the pitch of 46.062 Å, as shown in Fig. 2b.

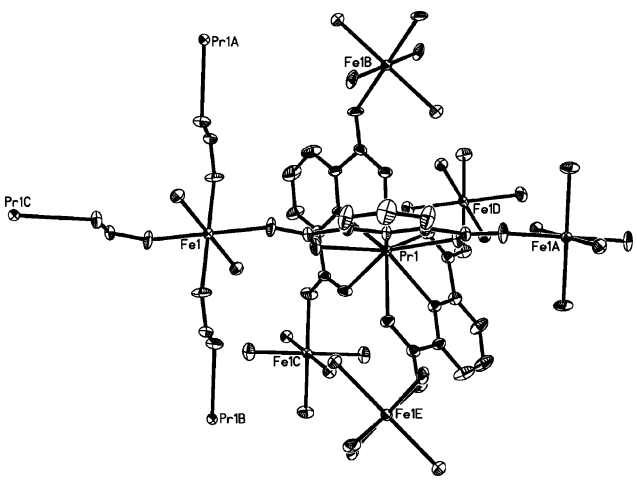

Fig. 1 Diagram showing the coordination environment of Fe^{II}_{HS}, Pr^{III} ions and the building units in **1**. H atoms are omitted for clarity. Symmetry codes: A: –y+1, x–y, z; B: –x+y+1, –x+1, z; C: –y+1, –x+1, –z+1/2; D: –x+y+1, y, –z+1/2; E: x, x–y, –z+1/2.

Interestingly, the lattice water molecules are trapped in 1D channels of **1–17** (Fig. 3), and construct two types of "water" pipes: type I, a centered single-wall "water" pipe (Fig. 3a); type II, a hollow single-wall "water" pipe (Fig. 3b), summarized in Table 4. Type I and II "water" pipes have been found in the analogous Mn–Ln polymers.[10e,g] In [Fe^{II}_{HS}–L^1–Ln^{III}] and [Co^{II}–L^1–Ln^{III}] coordination polymers, **1–3**, **8–14** and **16** contain type I "water" pipes, while **4–6**, **15** and **17** contain type II ones. The "water" pipe in the 1D channel is stabilized by hydrogen bonds between water molecules in the outer-wall pipe and the coordinated water molecules on Fe^{II}_{HS}/Co^{II} ions. Although there are a lot of water polymers encapsulated in the void spaces of coordination polymers reported,[30] this phenomenon, presenting two types of "water" pipes in one structural system, is very rare.

Table 4 Summary of "water" pipes in [Fe^{II}_{HS}–L^1–Ln^{III}] and [Co^{II}–L^1–Ln^{III}] series (**1–17**) (except for **7**)

[Fe^{II}_{HS}–L^1–Ln^{III}]	**1**	**2**	**3**	**4**	**5**	**6**	**8**	**9**
Type of "water" pipe (top)	I	I	I	II	II	II	I	I
Type of "water" pipe (bottom)	I	I	I	I	I	II	I	II
[Co^{II}–L^1–Ln^{III}]	**10**	**11**	**12**	**13**	**14**	**15**	**16**	**17**

As shown in Table 5, the bond length of Fe–O_W is longer than that of Fe–O_C in the corresponding polymer, and then the coordination geometry of Fe^{II}_{HS} ion is an elongated octahedron. The Ln–O_C and Ln–N distances (except for **8**) decrease with the decreasing radii of Ln^{III} ion due to the lanthanide contraction effect, as do the Fe···Fe, Fe···Ln, Ln···Ln nonbonding separations and the diameters of 1D channels (except for **3** and **5**). The similar phenomena is observed in the series of [Co^{II}–L^1–Ln^{III}] coordination polymers with some irregularity (Table 6).

Structural description of [Co^{II}–L^2–Ln^{III}] coordination polymers

While we investigated the coordination chemistry of H_3L^2 with Co^{II} and Ln^{III}, a series of isostructural [Co^{II}–L^2–Ln^{III}] coordination polymers (**18–25**) were obtained. **18–25** crystallize in monoclinic system $P2_1/c$ space group and display 2D-layer structures based on double-stranded helical motifs. Some of the coordinated water molecules in those polymers show a certain extent of disorder, which may originate from the poor single crystal quality. Here, the 2D-layer structure, represented by **18**, is depicted in detail. As shown in Fig. 4, there are two crystallographically independent Co^{II} ions, one Eu^{III} ion, one L^2 anion, two HL^2 anions and seven coordinated water molecules. Both Co1 and Co2 ions are six-coordinated with O atoms to form distorted octahedral geometries. The coordination environment of Co1 consists of one hydroxyl group, two carboxylic O atoms and three water molecules, while that of Co2 is constructed of two carboxylic O atoms and four water molecules. Eu1 center is nine-coordinated with a tricapped trigonal prismy geometry, and surrounded by one L^2 and two HL^2 anions in tridentate chelated mode. L^2 and HL^2 anions show different bonding modes to connect metal ions, L^2 adopts tridentate mode, while HL^2 with bidentate and tridentate modes (Scheme 2). As a result, each Eu1 center connects five Co ions (three Co1 and two Co2) through four carboxyl groups and one L^2 anions, while Co1 and Co2 have three and two Eu1 ions as the nearest neighbors, respectively.

Ignoring the bonding of hydroxyl group, Co^{II} ions are bridged by carboxyl groups to form a right-/left-hand (**P**/**M**) double-stranded helix with a pitch of 17.95 Å, while Eu^{III} ions act as

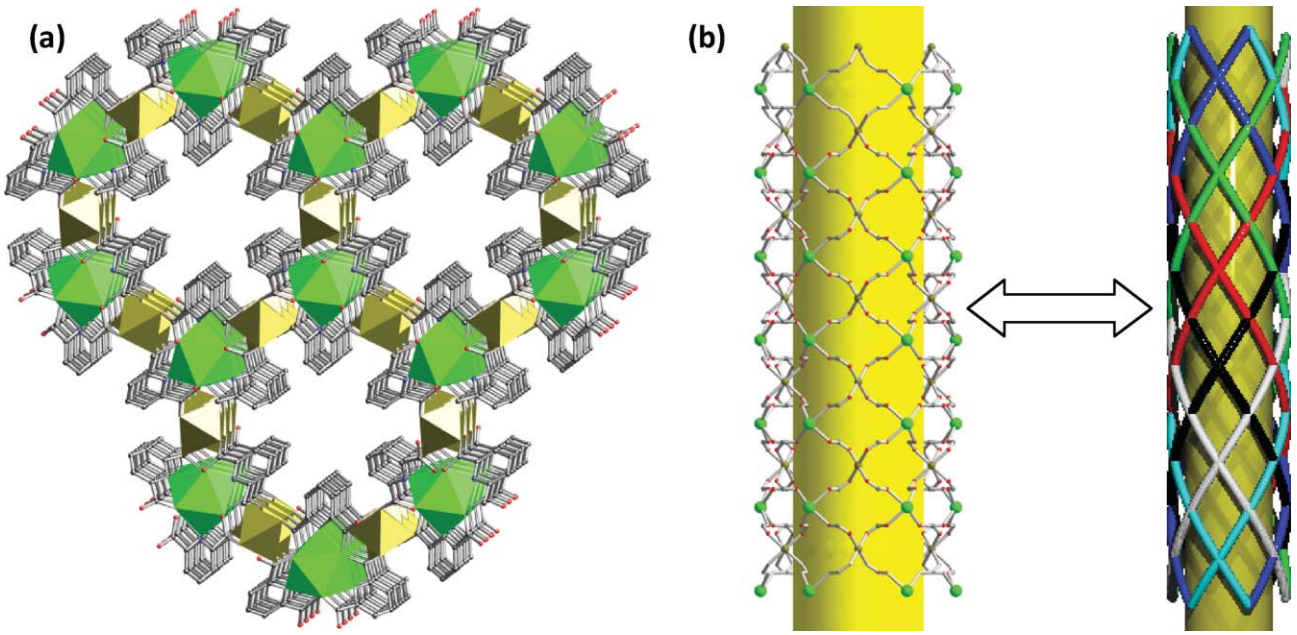

Fig. 2 (**a**) The 3D porous structure showing 1D channel along *c* direction in **1**; (**b**) the wall of 1D channel consisted of interweaving left- and right-hand sextuple-stranded helixes. H, some C and N atoms are omitted for clarity. Green polyhedra, [PrN_3O_6]; bronze polyhedra, [FeO_6]; gray, C; blue, N; red, O.

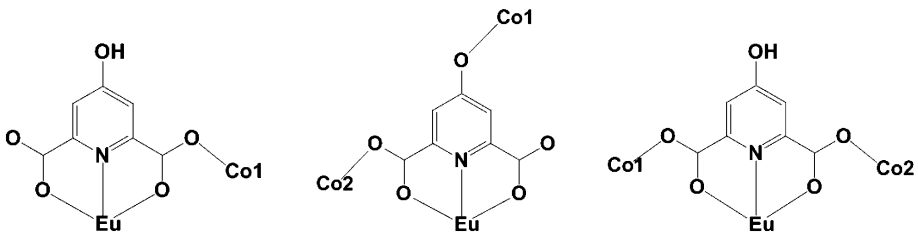

Scheme 2 Coordination modes of L2 and HL2 anions in **18**.

Table 5 Average bond lengths and metal···metal distances (Å) for **1–9** (except for **7**)

	1	**2**	**3**	**4**	**5**	**6**	**8**	**9**
Fe–O_W	**2.199**	**2.181**	**2.211**	**2.215**	**2.194**	**2.202**	**2.207**	**2.215**
Fe–O_C	**2.112**	**2.098**	**2.100**	**2.098**	**2.100**	**2.092**	**2.084**	**2.081**
Ln–O_C	**2.497**	**2.484**	**2.468**	**2.444**	**2.442**	**2.433**	**2.416**	**2.428**
Ln–N	**2.578**	**2.548**	**2.530**	**2.496**	**2.500**	**2.483**	**2.462**	**2.456**
Fe···Fe	7.757	7.665	7.702	7.619	7.646	7.600	7.593	7.583
Fe···Ln	5.899	5.866	5.891	5.890	5.886	5.869	5.870	5.882
Ln···Ln	8.857	8.851	8.895	8.798	8.829	8.776	8.767	8.755
Diameter of 1D channel	**17.91**	**17.70**	**17.79**	**17.60**	**17.68**	**17.55**	**17.54**	**17.51**

O_W, oxygen atom of the coordination water; O_C, oxygen atom of the carboxyl group.

Table 6 Average bond lengths and metal···metal distances (Å) for **10–17**

	10	**11**	**12**	**13**	**14**	**15**	**16**	**17**
Co–O_W	2.148	2.149	2.145	2.154	2.152	2.173	2.170	2.165
Co–O_C	2.081	2.080	2.071	2.071	2.073	2.082	2.065	2.053
Ln–O_C	2.499	2.484	2.453	2.449	2.443	2.449	2.425	2.397
Ln–N	2.582	2.560	2.531	2.509	2.493	2.502	2.473	2.427
Co···Co	7.750	7.717	7.655	7.640	7.606	7.644	7.610	7.507
Co···Ln	5.872	5.867	5.852	5.854	5.849	5.884	5.854	5.833
Ln···Ln	8.948	8.909	8.838	8.821	8.782	8.826	8.787	8.669
Diameter of 1D channel	17.90	17.82	17.68	17.64	17.57	17.65	17.57	17.34

O_W, oxygen atom of the coordination water; O_C, oxygen atom of the carboxyl group.

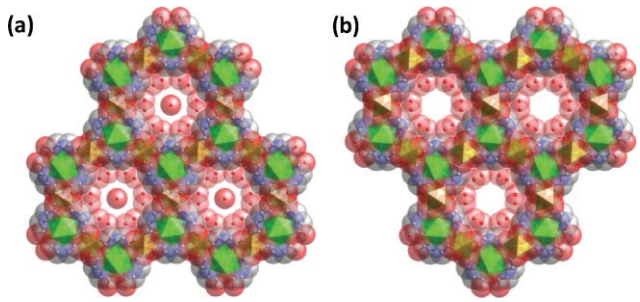

Fig. 3 The 3D porous structure of **1–17** accommodating two types of "water" pipes (**a**, type I; **b**, type II)in the 1D channels. H and some C atoms are omitted for clarity. Green polyhedra, [LnN_3O_6]; bronze polyhedra, [FeO_6] or [CoO_6]; gray, C; blue, N; red, O.

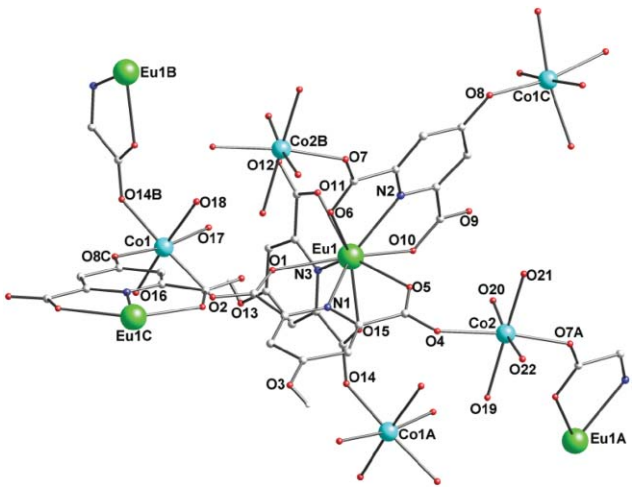

Fig. 4 Coordination environments of Co^{II} and Eu^{III} ions in **18**. Some H atoms are omitted for clarity. Symmetry codes A: x–1, y, z; B: x+1, y, z; C: x+1, –y+3/2, z+1/2.

nodes, as shown in Fig. 5a. **P**- and **M**-helixes are connected alternately by Co1–O_H bonds to form a 2D layer (Fig. 5b), which exhibits the achirality of this polymer, confirmed by the result of single-crystal X-ray analysis. Furthermore, the uncoordinated hydroxyl groups provide rich hydrogen bonding donors, while the coordinated hydroxyl oxygen atoms act as acceptors, and then the 2D layer is further assembled into a 3D porous structure with 1D channels along the *a* direction (Fig. 5c). The separation of O···O is 2.639 Å with angle of O–H···O of 177.90°, and the details of intermolecular hydrogen bonds associated with [Co^{II}–L^2–Ln^{III}] coordination polymers are listed in Table 7.

The lattice water molecules in **18** construct an infinite "water" tape through hydrogen bonds along the *a* direction, and the repeated unit is a $(H_2O)_{18}$ cluster involving a $(H_2O)_{12}$ cycle (Fig. 6a). The "water" tape is only well defined in **18**, whereas in **19–25** the water content was found to vary and the electron density in the channels was found to be quite diffuse making it difficult to locate water molecules unambiguously so that only the major water sites were included in the models. The O···O distances are in the range of 2.742–3.054 Å, comparable to 2.759 Å in ice I_h and 2.85 Å in liquid water.[31] Each 1D channel is threaded by a "water" tape, resulting in a host–guest 3D framework (Fig. 6b). Meanwhile, the water molecules in the "water" tapes are further stabilized by hydrogen bonding interactions with the channel, and the shape of the "water" tape closely follows that of the host channel, indicating a complimentary relationship between the guest and host in **18**.

The average bond lengths associated with Co and Ln atoms (Å) in the series of [Co^{II}–L^2–Ln^{III}] coordination polymers are listed in Table 8. The Co–O_C distance is much longer than that of Co–O_W or Co–O_H, and the bond length of Co–O_H is the shortest one in the corresponding polymers. The Ln–O_C and Ln–N distances decrease with the decreasing lanthanide ionic radii in the whole series, although with some irregularity.

In the previous work of our group, the combination of H_3L^2 with Mn^{II}/Zn^{II} and Ln^{III} resulted in 2D honeycomb-type Mn/Zn–Ln coordination polymers,[10g,17c] in which, all the hydroxyl groups did not coordinate to metal ions and were directed towards to the center of the cavity, resulting in a honeycomb structure with C_3 symmetry. The structure of [Co^{II}–L^2–Ln^{III}] coordination polymers is a 2D layer constructed through coordination bonds, while partial hydroxyl groups coordinate to Co^{II} ions, which is completely different from those of Mn/Zn–Ln coordination polymers, and the coordinated and uncoordinated hydroxyl groups in [Co^{II}–L^2–Ln^{III}] coordination polymers provide rich hydrogen bonds, which link the 2D layers into a 3D porous network.

Thermogravimetric and elemental analyses

For the series of [Fe^{II}_{HS}–L^1–Ln^{III}], [Co^{II}–L^1–Ln^{III}] and [Co^{II}–L^2–Ln^{III}] coordination polymers are isostructural, respectively, **2**, **12** and **23** were selected for thermogravimetric analyses (TGA) to examine the thermal stability of the present structures. TGA curves for **2**, **12** and **23** are shown in Fig. 7. The results of **2** and **12** are very similar for their isomorphous structures, and show two steps of weight loss below 300 °C. The first weight loss occurred in the range of 25–140 °C, corresponding to the uncoordinated water molecules, which includes the lattice and adsorbed water molecules. Taking account of the large pores in [Fe^{II}_{HS}–L^1–Ln^{III}] and [Co^{II}–L^1–Ln^{III}] series, **2** and **12** possibly adsorb some water molecules at room temperature, which is also confirmed by the elemental analyses (Table 1). Each molecule in the [Fe^{II}_{HS}–L^1–Ln^{III}] and [Co^{II}–L^1–Ln^{III}] series adsorbs some molecules to achieve saturation, the difference between [Fe^{II}_{HS}–L^1–Ln^{III}] and [Co^{II}–L^1–Ln^{III}] series is the number of uncoordinated water molecules at saturation: eight for [Fe^{II}_{HS}–L^1–Ln^{III}] and nine for [Co^{II}–L^1–Ln^{III}]. We chose the [Fe^{II}_{HS}–L^1–Ln^{III}] series to do the comparable experiments, and the elemental analysis of **2** is performed on the crystalline samples without drying, while others are performed after vacuum drying. The results of elemental

Table 7 The O···O distances and angles of O–H···O of intermolecular hydrogen bonds for **18–25**

	18	**19**	**20**	**21**	**22**	**23**	**24**	**25**
O···O distance (Å)	2.639	2.634	2.631	2.652	2.637	2.642	2.648	2.644
O···H–O angle (°)	171.09	168.14	172.09	163.12	168.09	174.60	176.45	175.86

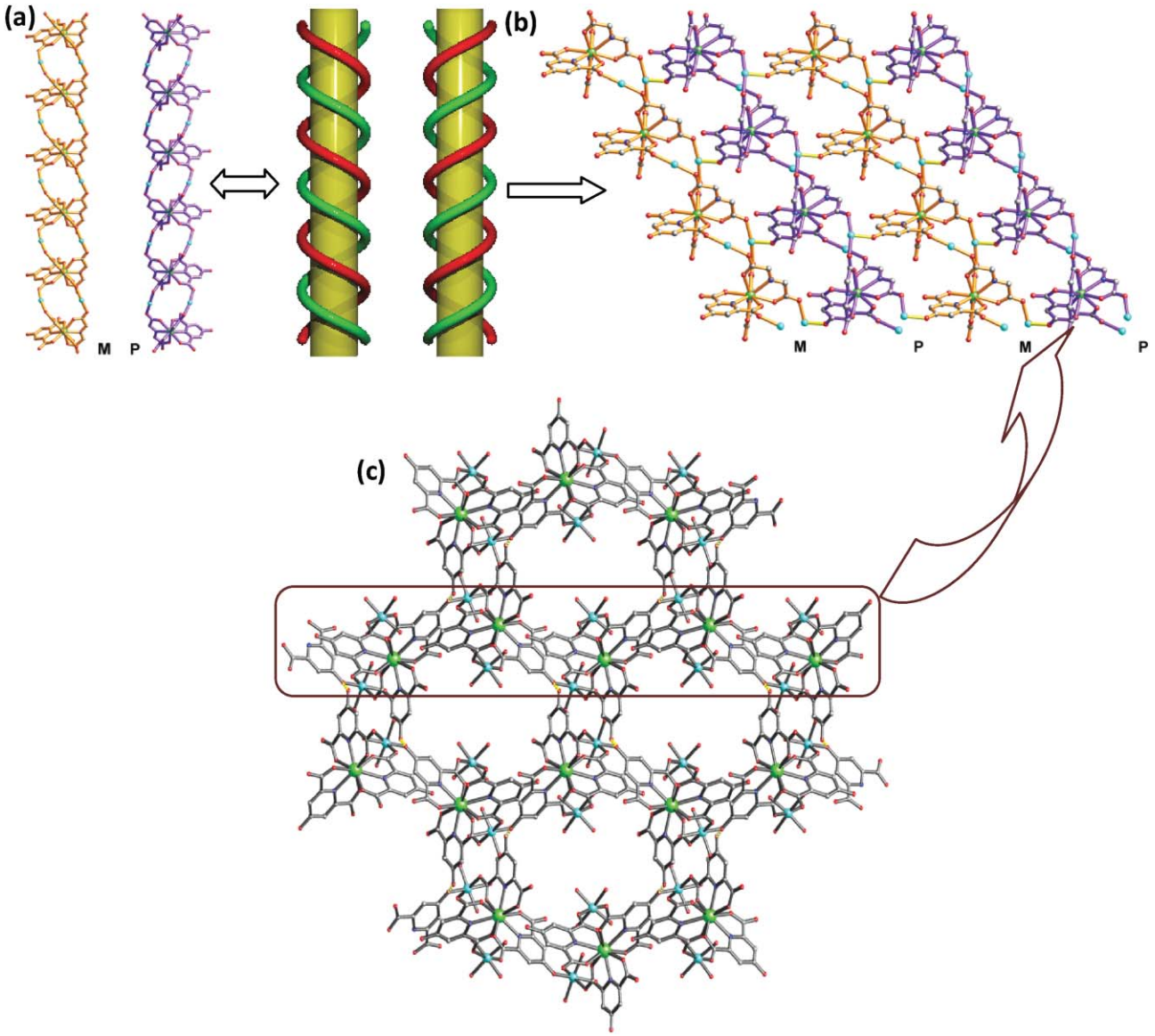

Fig. 5 (**a**) The right- and left-hand double-stranded helical motifs; (**b**) the 2D layer based on double-stranded motifs; (**c**) the 3D porous framework constructed by 2D layers with strong intermolecular hydrogen bonds.

Table 8 Average bond lengths associated with Co^{II} and Ln^{III} centers (Å) for **18–25**

	18	**19**	**20**	**21**	**22**	**23**	**24**	**25**
Co1–O_W	2.081	2.076	2.064	2.111	2.069	2.092	2.060	2.061
Co1–O_C	2.191	2.202	2.185	2.199	2.181	2.183	2.186	2.183
Co1–O_H	2.036	2.043	2.062	2.067	2.062	2.058	2.046	2.052
Co2–O_W	2.062	2.056	2.046	2.090	2.060	2.085	2.057	2.054
Co2–O_C	2.142	2.169	2.137	2.179	2.144	2.155	2.120	2.129
Ln–O_C	2.406	2.422	2.379	2.416	2.379	2.367	2.367	2.358
Ln–N	2.477	2.505	2.453	2.516	2.465	2.455	2.443	2.432

O_W, oxygen atom of the coordinated water molecule; O_C, oxygen atom of the carboxyl group; O_H, oxygen atom of the hydroxyl group.

analyses display that this kind of structure can adsorb water molecules at room temperature to satisfy the demands of the pores (Table 1).

The first weight losses are 8.73% for **2** (calculated 8.57% for **2**·H_2O) and 9.38% for **12** (calculated 9.32% for **12**·$2H_2O$), indicative of adsorbing one water molecule per [Fe_3Nd_2] unit of **2** and two water molecules per [Co_3Sm_2] unit of **12**. Namely, the first weight losses for **2** and **12** correspond to uncoordinated and adsorbed water molecules, which are confirmed by the elemental analyses (Table 1). The second weight loss of 6.51% and 6.24%

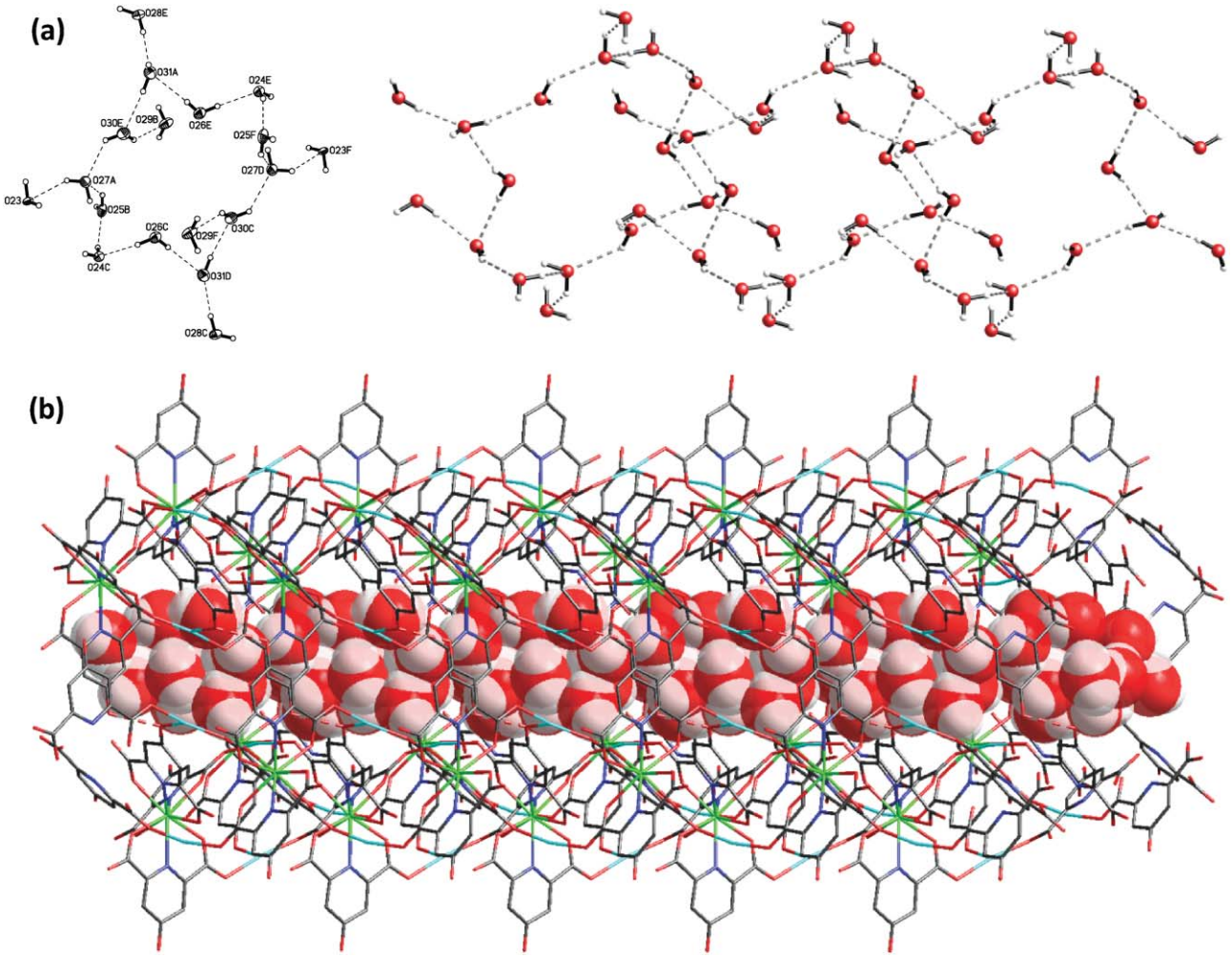

Fig. 6 (**a**) The 1D water tape with repeated $(H_2O)_{18}$ motif in **18**; (**b**) the side-view of the 1D channel with accommodating water tape in **18**.

from 140–300 °C corresponds to the loss of the water molecules coordinated to Fe^{II}_{HS} or Co^{II} ions, and the calculated values are 6.43% and 6.21% for **2** and **12**, respectively. The frameworks of **2** and **12** collapsed at 400 °C. For **23**, the weight loss between 25–250 °C is 24.28%, which can be ascribed to all water molecules (coordinated and uncoordinated). Above 300 °C, **23** was gradually decomposed into oxide.

X-ray electronic spectroscopy (XPS)

From single-crystal X-ray diffraction analyses and charge balance consideration, Fe centers should be divalent in **1–9**. X-ray electronic spectroscopy (XPS) has been recorded at room temperature on crystalline sample of **9** to determine the oxidation state of Fe centers (see ESI†). The peak at 708.6 eV corresponds to the Fe(2p) binding energy, which matches well with the literature value of Fe^{II},[32] proving that the Fe center in **9** is Fe^{II} but not Fe^{III}.

Mössbauer spectroscopy

Although the single-crystal data and XPS show that Fe centers in [Fe^{II}–L^1–Ln^{III}] coordination polymers are divalent, in order to further determine the oxidation and spin state of Fe centers in these coordination polymers, **2** was chosen as an example to study the Mössbauer spectroscopy. The Mössbauer spectra of **2** have been recorded at 298 and 82 K (Fig. 8) on crystalline samples, respectively, and both consist of a quadrupole-split doublet. At 298 K, the doublet of isomer shift value δ = 1.27 mm s^{-1} and quadrupole-splitting value ΔE_Q = 1.71 mm s^{-1} with a fairly narrow linewidth Γ = 0.14 mm s^{-1} is typical of high-spin divalent Fe atoms,[33] while the observed doublet at 82 K with δ = 1.39 mm s^{-1}, ΔE_Q = 2.25 mm s^{-1} and Γ = 0.18 mm s^{-1}. Overall, these results indicate an S = 2 high-spin ground state Fe^{II} ion of **2** in the temperature range from 82 to 298 K, and the increase of the quadrupole splitting at low temperature may be ascribed to the population of the first excited state of Fe^{II} ion.

Luminescence properties

Considering the excellent luminescent properties of Sm^{III}, Eu^{III}, Tb^{III} and Dy^{III} ions, the luminescences of eight polymers in the [Fe^{II}_{HS}–L^1–Ln^{III}] and [Co^{II}–L^1–Ln^{III}] series were studied at room temperature, as shown in Fig. 9 and 10, respectively. Fig. 9 displays the emission spectra associated with Sm^{III}, Eu^{III}, Tb^{III} and Dy^{III}

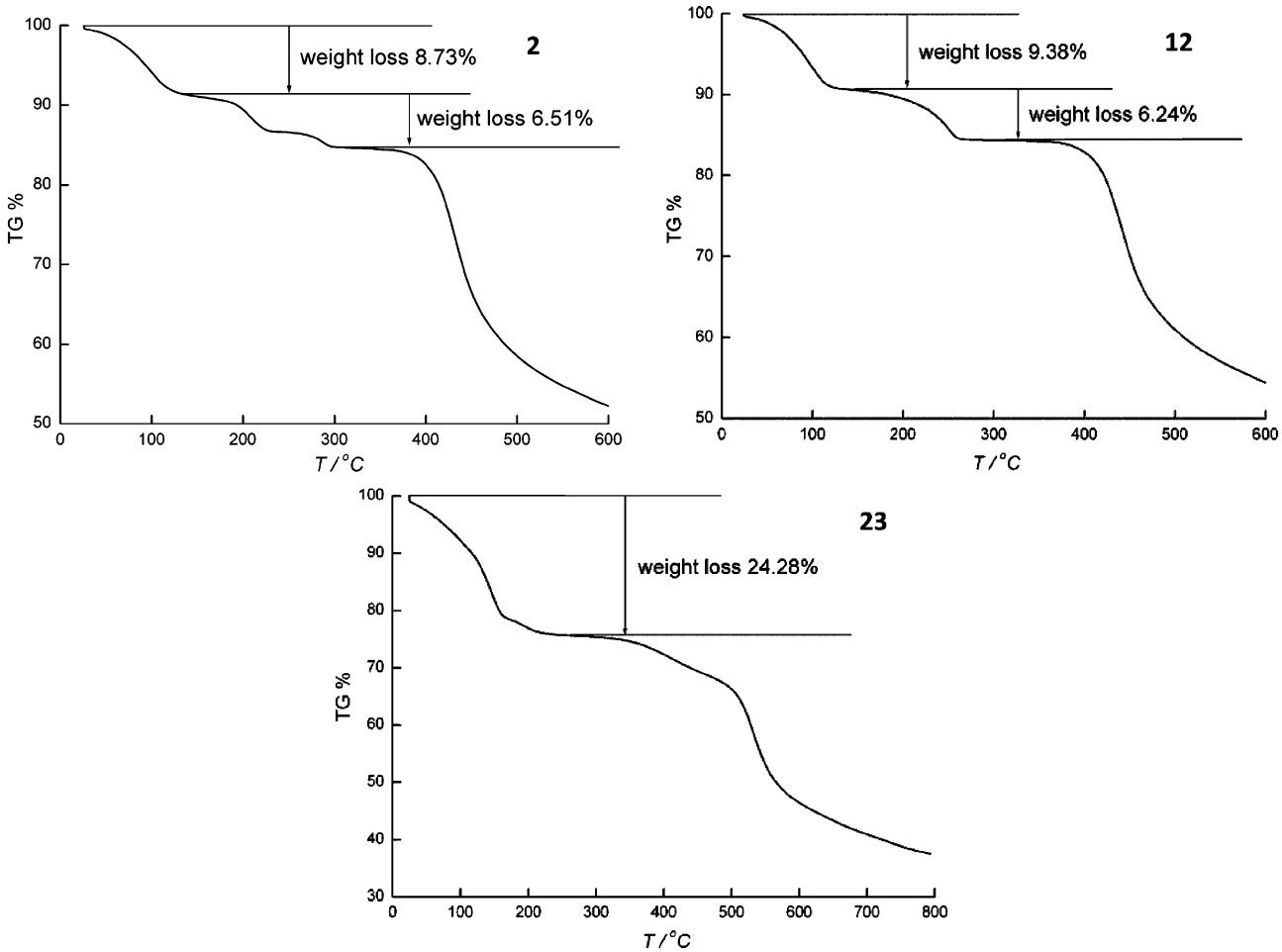

Fig. 7 TGA curves for **2**, **12** and **23**.

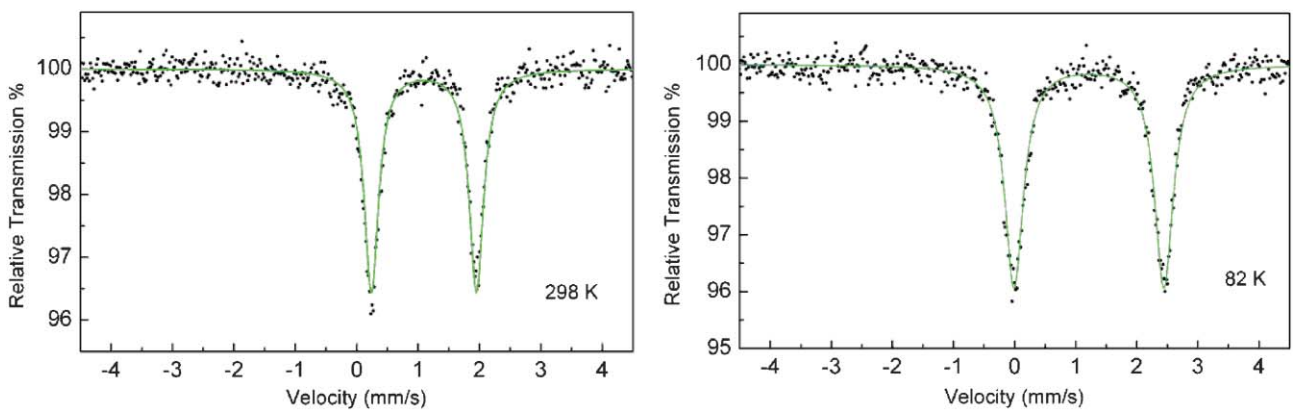

Fig. 8 The Mössbauer spectra of **2** at 298 K (left) and at 82 K (right). Solid lines are theoretical simulations assuming quadrupole doublets.

ions in [Fe^{II}_{HS}–L^1–Ln^{III}] series, and Fig. 10 with those in [Co^{II}–L^1–Ln^{III}] series.

When excited at 312 nm, **3** in DMF exhibits a broad strong peak around 450 nm, which can be ascribed to the intraligand transition of L^1, and the typical emission of Sm^{III} ion is present at 562, 598 and 645 nm, corresponding to $^4G_{5/2}\rightarrow{}^6H_{5/2}$, $^4G_{5/2}\rightarrow{}^6H_{7/2}$ and $^4G_{5/2}\rightarrow{}^6H_{9/2}$ transitions, respectively.[34] The $^4G_{5/2}\rightarrow{}^6H_{7/2}$ transition is broad with a shoulder peak, indicating the transitions from $^4G_{5/2}$ to Stark sublevels split by $^6H_{7/2}$. The emission spectrum of **4** in DMF obtained upon irradiation at 304 nm is dominated by the intense hypersensitive Eu^{III} ($^5D_0\rightarrow{}^7F_2$) transition at 613 nm, and that of **6** upon 316 nm is dominated by the Tb^{III} ($^5D_4\rightarrow{}^7F_5$) transition at 546 nm, which have been reported previously, and it was found that **4** can act as a luminescent probe for Mg^{2+}.[28a] For

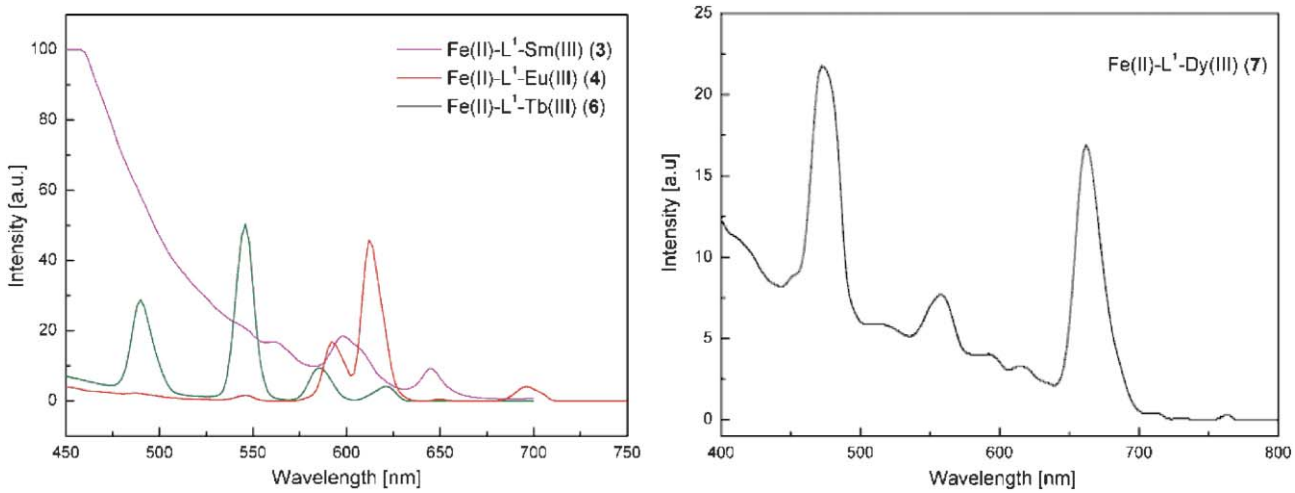

Fig. 9 Emission spectra of **3**, **4** and **6** in DMF (left) and **7** in solid state (right) at room temperature.

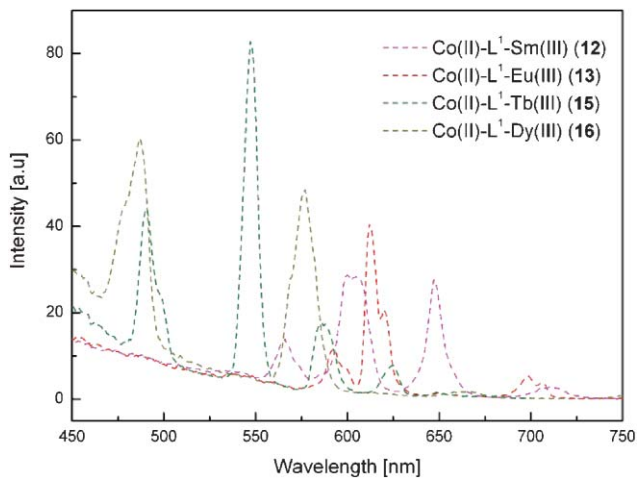

Fig. 10 Emission spectra of **12**, **13**, **15** and **16** in DMF at room temperature.

7, we did not observe the luminescence in DMF, and the emission spectrum in the solid state is depicted in Fig. 9 right. **7** displays the typical Dy^{III} emission at 474, 560 and 662 nm, attributed to the characteristic emission of $^4F_{9/2}\rightarrow{}^6H_J$ (J = 15/2-11/2) transitions, respectively.[35] The L^1-base emission is not observed in **4**, **6** and **7**, and the intense emission indicates the efficient energy transfer from L^1 to Eu^{III}, Tb^{III} and Dy^{III} centers.

12 emits the typical Sm^{III} luminescence excited at 270 nm, and exhibits the characteristic transitions of $^4G_{5/2}\rightarrow{}^6H_J$ (J = 5/2-11/2) at 566, 600, 647 and 710 nm, respectively.[34] The same with that of **3**, the $^4G_{5/2}\rightarrow{}^6H_{7/2}$ transition is split into two peaks, indicative of the transitions from $^4G_{5/2}$ to Stark sublevels. The emission spectrum of **13** in DMF arises from $^5D_0\rightarrow{}^7F_J$ (J = 1–4) under excited at 280 nm, typical of Eu^{III} ion: $^5D_0\rightarrow{}^7F_1$ (593 nm), $^5D_0\rightarrow{}^7F_2$ (612 nm), $^5D_0\rightarrow{}^7F_3$ (650 nm), $^5D_0\rightarrow{}^7F_4$ (698 nm).[36] The most intense emission is the $^5D_0\rightarrow{}^7F_2$ transition, which arises from the electric dipole moment and is hypersensitive to the environment of the Eu^{III} ion. The $^5D_0\rightarrow{}^7F_1$ transition from magnetic dipole is also present, and is less intense than $^5D_0\rightarrow{}^7F_2$, indicating the absence of inversion symmetry at the Eu^{III} center.[37] Obviously, all the transitions are broadened with shoulder peaks, and this can be ascribed to the splitting of ^7F_J on the effect of crystal-field. For **15**, when excited at 280 nm, the characteristic Tb^{III} centered transition peaks are observed at 491, 545, 586 and 624 nm ascribed to $^5D_4\rightarrow{}^7F_J$ (J = 6–3), respectively. The dominant emission is $^5D_4\rightarrow{}^7F_5$ transition, which gives an intense green luminescence.[38] When **16** in DMF was excited at 280 nm, it gave a typical Dy^{III} emission spectrum. Two dominant emissions at 487 and 577 nm correspond to $^4F_{9/2}\rightarrow{}^6H_{15/2}$ and $^4F_{9/2}\rightarrow{}^6H_{13/2}$ transitions, respectively, and the weak emission at 663 nm is ascribed to the $^4F_{9/2}\rightarrow{}^6H_{11/2}$ transition.[35] The absence of the L^1-based emission in the spectra of **12**, **13**, **15** and **16** suggests the effective energy transfer from L^1 to Ln^{III} centers. Inspired by the luminescent selectivity of **4** for Mg^{2+}, we wondered whether polymers in the [Co^{II}–L^2–Ln^{III}] series would provide potential candidates for luminescent probe of divalent metal ions. Thus, the introduction of metal ions (such as Mg^{2+}, Zn^{2+}, Cd^{2+}, Mn^{2+}, Ca^{2+}) into **12**, **13**, **15** and **16** systems are carried out, which leads to weakening or even quenching of the lanthanide luminescence of corresponding system, and no luminescent probe is found (see ESI).

The luminescent properties of isomorphous [Fe^{II}_{HS}–L^1–Ln^{III}] and [Co^{II}–L^1–Ln^{III}] series show differences: i) the emission spectrum of [Fe^{II}_{HS}–L^1–Sm^{III}] (**3**) displays strong intraligand transition, while that of [Co^{II}–L^1–Sm^{III}] (**12**) does not exhibit this transition, indicative of the inefficient energy transferring from L^1 to Sm^{III} ion, and then result in the strong intraligand transition of L^1; ii) [Fe^{II}_{HS}–L^1–Eu^{III}] (**4**) displays luminescent selective detection of Mg^{2+}, and no polymer in [Co^{II}–L^1–Ln^{III}] series acts as luminescent probes; iii) for [Fe^{II}–L^1–Dy^{III}] (**16**), there is no emission peak observed in DMF, which maybe attribute to the effect of solvent or Fe^{II}_{HS} ion to the luminescence of Dy^{III} ion in DMF. Considering the [Mn^{II}–L^1–Ln^{III}] analogous, the [Mn^{II}/Fe^{II}_{HS}/Co^{II}–L^1–Ln^{III}] systems display significant differences in luminescent selectivity for bivalent metal ions (such as Zn^{2+}, Mg^{2+}) (Table 9), in which [Mn^{II}–L^1–Eu^{III}/Tb^{III}] act as luminescent probe for Zn^{2+},[10f] and [Mn^{II}–L^1–Dy^{III}] for Mg^{2+},[10g] [Fe^{II}_{HS}–L^1–Eu^{III}] shows luminescent selective detection of Mg^{2+},[28a] and none of [Co^{II}–L^1–Ln^{III}] exhibits this behavior (see ESI). As some reports have depicted that the luminescence arising from the lanthanide ions was directly modulated by the presence of the *d*-metal ions in solution,[39] it is possible that *d*-metal ions in *d*-*f* systems have the same

Table 9 Effect of Zn^{2+} and Mg^{2+} on the luminescent intensity of [Mn^{II}–L^1–Ln^{III}], [$Fe^{II}{}_{HS}$–L^1–Ln^{III}] and [Co^{II}–L^1–Ln^{III}] series ('↑', increase; '↓', decrease; '=', equal)

	Mn–Eu	Fe–Eu	Co–Eu	Mn–Tb	Fe–Tb	Co–Tb	Mn–Dy	Co–Dy
Zn^{2+}	↑	↓	↓	↑	↓	↓	↓	↓
Mg^{2+}	↓	↑	=	↓	=	=	↑	↓
Luminescent selectivity	Zn^{2+}	Mg^{2+}		Zn^{2+}			Mg^{2+}	

behavior to modulate the luminescence of lanthanide ions. Viewing the structural characteristics, [Mn^{II}/$Fe^{II}{}_{HS}$/Co^{II}–L^1–Ln^{III}] systems display similar 3D porous networks with 1D nanotubes, when the lanthanide ions are uniform, and the difference among the networks is *d*-metal ions. For example, [Mn^{II}–L^1–Eu^{III}],[10f] [$Fe^{II}{}_{HS}$–L^1–Eu^{III}] (**4**) and [Co^{II}–L^1–Eu^{III}] (**13**) polymers contain the same Ln^{III} ions, while the *d*-metal ions in their networks are Mn^{II}, $Fe^{II}{}_{HS}$ and Co^{II}, respectively. The luminescent intensity of [Mn^{II}–L^1–Eu^{III}] increases significantly upon adding Zn^{2+} and decreases upon adding Mg^{2+}, showing luminescent selectivity for Zn^{2+}, and [$Fe^{II}{}_{HS}$–L^1–Eu^{III}] (**4**) displays the contrary behavior with luminescent selectivity for Mg^{2+}, while that of [Co^{II}–L^1–Eu^{III}] (**13**) decreases and maintains upon adding Zn^{2+} and Mg^{2+}, respectively. The results indicated that the *d*-metal ions (Mn^{II}, $Fe^{II}{}_{HS}$ and Co^{II}) in the networks may play an important role in the luminescent selectivity of [Mn^{II}/$Fe^{II}{}_{HS}$/Co^{II}–L^1–Ln^{III}] systems for different guest ions.

We also investigated the luminescence of [Co^{II}–L^2–Ln^{III}] coordination polymers (**18**, **20** and **21**), however, the luminescence of lanthanide ions is quenched, either in DMF or in solid state, which maybe ascribe to the HO-substituted effect and/or the modulation of Co^{II} ions to the luminescence of lanthanide ions.

Magnetic properties

The magnetic properties of heterometallic coordination polymers with lanthanide have been rarely investigated, due to the unquenched first-order orbital momentum of lanthanide ions (except for Gd^{III}) under ligand-field effect. It is noted that the $4f^n$ configuration of Ln^{III} ion is split into $^{2S+1}L_J$ states by the interelectronic repulsion and spin–orbit coupling. Further splitting into Stark components ($2J + 1$ if n is even, $J + 1/2$ if n is odd) is caused by the crystal-field perturbation, which depends on the symmetry site of the ion.[40] Except for Sm^{III} and Eu^{III}, the $^{2S+1}L_J$ ground state is well separated from the first excited state. At room temperature, all the Stark levels arising from the n-fold degenerate $^{2S+1}L_J$ ground state of Ln^{III} ion, except Gd^{III} ion with an f^7 electronic configuration, are thermally populated. As the temperature is lowered, a progressive depopulation of these Stark sublevels takes place. When combined with *d*-metal ions, it is more complicated to interpret the magnetic nature between *d*- and *f*-metal ions, especially in multi-dimensional *d*–*f* structures, because the single ion behavior of *f*- and some *d*-metal (*e.g.* Co^{II}) ions maybe shield the antiferromagentic or weak ferromagnetic coupling nature between them. Despite these aspects, heterometalllic *d*–*f* coordination polymers are of high interest in molecular magnetism, and we investigate the magnetic interaction between Mn^{II} and Ln^{III} ions in [Mn^{II}–L^2–Ho^{III}/Er^{III}] coordination polymers using Zn^{II}-diamagnetic ions substitution.[17c] Here we study the magnetic properties of these Fe/Co–Ln coordination polymers to make contributions to understand the magnetic interactions in *d*–*f* systems.

The temperature-dependent magnetic susceptibility data of polycrystalline samples of **3**, **6**, **7**, **9**, **13**, **15–17** and **19–24** have been recorded at an applied magnetic field of 1000 Oe in the temperature range of 2–303/300 K. The predicted and measured $\chi_M T$ values at room temperature and 2 K are detailed in Table 10.

The plots of $\chi_M T$ *versus* T for **3**, **6**, **7** and **9** in [$Fe^{II}{}_{HS}$–L^1–Ln^{III}] series are shown in Fig. 11, and the magnetic data also confirm the high-spin Fe^{II} ions. The profiles of plots show the same feature, that is, a decrease in the values of $\chi_M T$ with lowing temperature, indicating similar magnetic behavior. The observed $\chi_M T$ value at room temperature for each polymer is very close to the theoretical value calculated for three isolated high-spin Fe^{II} ($S = 2$) and two Ln^{III} ions in the ground states for **3** ($^6H_{5/2}$), **6** ($^7F_6$), **7** ($^6H_{15/2}$) and **9** ($^4I_{15/2}$), respectively (Table 10). When the temperature is lowered, the $\chi_M T$ values decrease slowly, until reaching minima at 2 K. This behavior may be due to the thermal depopulations of the Stark sublevels and/or exchange coupling between $Fe^{II}{}_{HS}$ and Ln^{III} ions, thus, we can not definitely explain that antiferromagnetic interactions occur between $Fe^{II}{}_{HS}$ and Ln^{III} ions only from the $\chi_M T$ values smoothly decreasing on cooling.

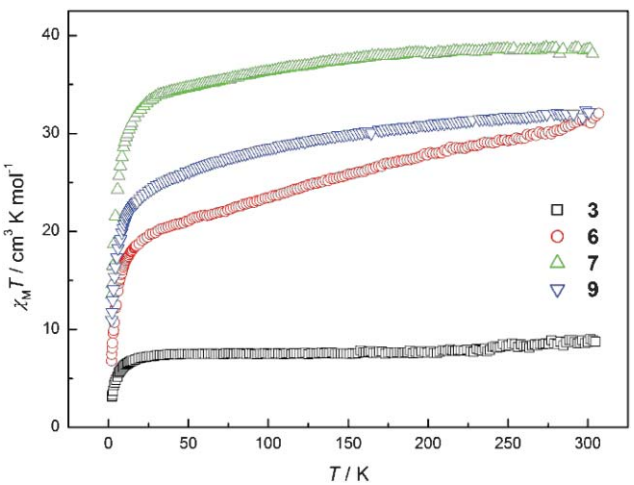

Fig. 11 Plots of $\chi_M T$ *versus* T for **3**, **6**, **7** and **9** in [$Fe^{II}{}_{HS}$–L^1–Ln^{III}] series.

Fig. 12 depicts the temperature dependence of the magnetic susceptibilities for **13** and **15–17** in the [Co^{II}–L^1–Ln^{III}] series. The experimental $\chi_M T$ value for **13** at room temperature (11.41 cm^3 K mol^{-1}) is much higher than the theoretical value (5.63 cm^3 K mol^{-1}) calculated for three uncoupled Co^{II} ions ($S = 3/2$) and two Eu^{III} ions in the ground state $^7F_0$, originating from the magnetic contribution of the lower excited state ^7F_J of Eu^{III} ions and the orbit angular momentum of high-spin Co^{II} ions in the octahedron.[41] The energy of the lower excited state ^7F_J is slightly higher than that of

Table 10 Magnetic data extracted from the plots of $\chi_M T$ vs. T (under 1000 Oe) and the predicted $\chi_M T$ values for **3**, **6**, **7**, **9**, **13**, **15–17** and **19–24**

	Calculated unit	$\chi_M T$ (cm^3 K mol^{-1}) predicted at RT	$\chi_M T$ (cm^3 K mol^{-1}) measured at 303 or 300 K	$\chi_M T$ (cm^3 K mol^{-1}) measured at 2 K
3	[Fe_3Sm_2]	9.18	9.02	3.13
6	[Fe_3Tb_2]	32.62	32.06	6.79
7	[Fe_3Dy_2]	37.36	38.17	13.57
9	[Fe_3Er_2]	31.94	32.16	10.97
13	[Co_3Eu_2]	8.64	11.41	4.74
15	[Co_3Tb_2]	29.24	30.63	7.67
16	[Co_3Dy_2]	33.96	35.17	19.73
17	[Co_3Yb_2]	10.78	12.73	5.81
19	[Co_2Gd]	11.69	12.98	8.82
20	[Co_2Tb]	15.56	16.54	6.17
21	[Co_2Dy]	17.93	18.92	14.19
22	[Co_2Ho]	17.82	18.64	5.02
23	[Co_2Er]	15.22	17.28	11.06
24	[Co_2Tm]	10.89	11.68	3.75

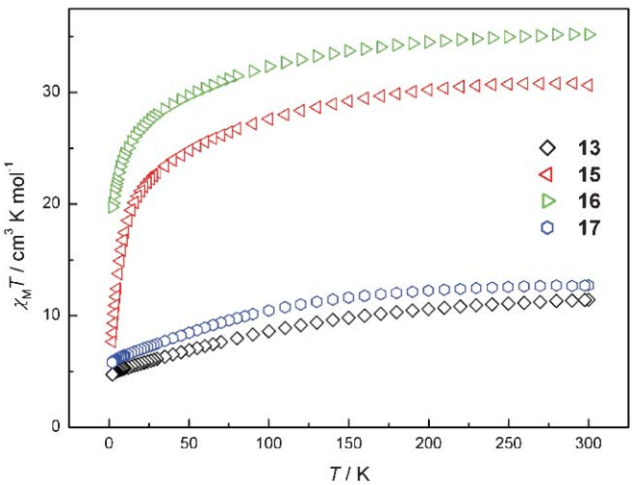

Fig. 12 Plots of $\chi_M T$ *versus* T for **13** and **15–17** in the [Co^{II}–L^1–Ln^{III}] series.

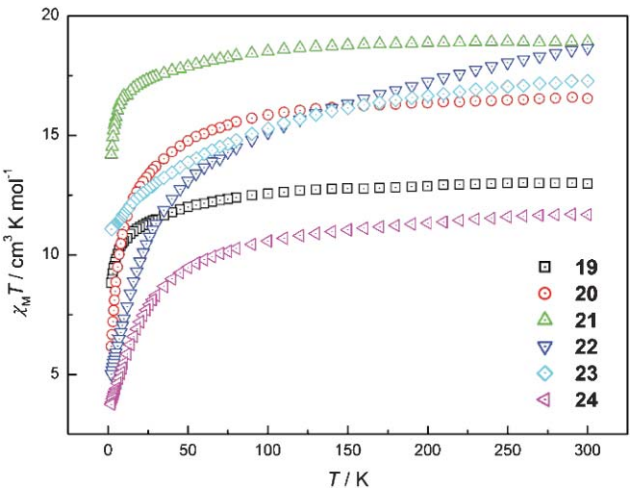

Fig. 13 Plots of $\chi_M T$ *versus* T for **19–24** in [Co^{II}–L^2–Ln^{III}] series.

the ground state $^7F_0$; at room temperature the lower excited state ^7F_J are thermally populated, and the contribution of the excited state can not be ignored. Therefore, the theoretical value of Eu^{III} ions should be calculated by the van Vleck equation allowing for population of lower excited state ^7F_J and the experiential $\chi_M T$ value of one uncoupled Eu^{III} ion is 1.5 cm^3 K mol^{-1}. The experimental $\chi_M T$ values for **15–17** at room temperature are slightly higher than the theoretical values calculated for three uncoupled high-spin Co^{II} ions (S = 3/2) and two Ln^{III} ions in the ground state for **15** ($^7F_6$), **16** ($^6H_{15/2}$) and **17** ($^2F_{7/2}$), respectively (Table 10), indicative of the typical contribution of the orbital momentum for the ground state $^4T_{1g}$ of Co^{II} ions.[41] The $\chi_M T$ values gradually decrease with the lowering temperature, reaching minima at 2 K, respectively. The decrease in $\chi_M T$ values with cooling might be attributed to the single ion behavior of high-spin Co^{II} and Ln^{III} ions because of strong spin–orbit coupling and/or the antiferromagnetic intereaction between Co^{II} and Ln^{III} ions. Thus, the nature of magnetic interactions between Co^{II} and Ln^{III} ions are not explicitly determined.

Fig. 13 shows the $\chi_M T$ *versus* T curves for **19–24**, and the trend of the magnetization curves are similar. The measured $\chi_M T$ values for **19–24** at room temperature are in good agreement with the expected values calculated for two isolated high-spin Co^{II} ions and one Ln^{III} ion, respectively (Table 10). As often reported in many Co^{II} containing compounds,[41] the $\chi_M T$ value at room temperature is usually higher than the expected spin-only one as a result of the orbital contribution of the high-spin Co^{II} to the magnetism. The $\chi_M T$ values for **19–24** decrease slowly with lowering temperature, and reach minima at 2 K, respectively. Despite the decrease of $\chi_M T$ values on cooling, the nature of magnetic interactions between Co^{II} and Ln^{III} ions cannot be interpreted as antiferromagnetic coupling because of the strong spin–orbit coupling of Co^{II} and Ln^{III} ions.

The magnetic behaviors of the *d*–*f*-metal system are complicated, due to the magnetic coupling of the paramagnetic transition-metal centers and strong spin–orbit coupling of the lanthanide ions under ligand-field effect, furthermore, all coordination polymers in this paper exhibit 2D or even 3D networks. Thus, the magnetic coupling interactions between *d*- and *f*-metal ions in the series of [Fe^{II}_{HS}–L^1–Ln^{III}], [Co^{II}–L^1–Ln^{III}] and [Co^{II}–L^2–Ln^{III}] coordination polymers are not explicitly characterized.

Conclusion

In summary, three series of 3*d*–4*f* heterometallic coordination polymers have been produced through selecting different *d*-metal ions or HO-substituted ligand. The reaction of Fe^{II}, Ln^{III} and H_2L^1 in CH_3CN/H_2O resulted in 3D porous [Fe^{II}_{HS}–L^1–Ln^{III}]

coordination polymers with 1D channels. When replacing high-spin Fe^{II} by Co^{II}, a series of isomorphic 3D [Co^{II}–L^1–Ln^{III}] coordination polymers are obtained, and the series of 2D [Co^{II}–L^2–Ln^{III}] coordination polymers based on double-stranded helical motifs are fabricated by HO-substituted ligand with Co^{II} and Ln^{III} ions. In addition, the 3D porous coordination polymers contain two kinds of "water" pipes accommodated in 1D channels, showing fantastic edifices. XPS, Mössbauer spectroscopy and magnetic data confirm the oxidation and spin-state of Fe centers. The luminescent properties of [M^{II}–L^1–Ln^{III}] are studied, and reveal that *d*-metal ions in the networks play an important role in the luminescent selectivity of [M^{II}–L^1–Ln^{III}] for different guest ions. The complexities of *d*- and *f*-metal ions make the magnetic coupling nature difficult to interpret, needing more efforts to understand the unfathomable field. This work gives some insight into the synthesis of *d*–*f* heterometallic coordination polymers with excellent luminescent properties and more effort will be devoted to this field for searching for multi-dimensional magnets.

Acknowledgements

This work was supported by the NSFC (20971074 and 90922032), FANEDD (200732), NCET-07-0463, the NSF of Tianjin (10JCZDJC21700), MOE (IRT-0927) and the State Key Project of Fundamental Research of MOST (2007CB815305).

References

1 (*a*) A. D. C. Noord, J. W. Kampf and V. L. Pecoraro, *Angew. Chem., Int. Ed.*, 2002, **41**, 4667; (*b*) Y. F. Zhou, M. C. Hong and X. T. Wu, *Chem. Commun.*, 2006, 135; (*c*) R. Gheorghe, P. Cucos, M. Andruh, J. P. Costes, B. Donnadieu and S. Shova, *Chem. Eur. J.*, 2006, **12**, 187.

2 (*a*) H. Kou, B. Zhou, S. Gao and R. Wang, *Angew. Chem., Int. Ed.*, 2003, **42**, 3288; (*b*) S. Tanase and J. Reedijk, *Coord. Chem. Rev.*, 2006, **250**, 2501.

3 (*a*) J. C. G. Bünzli and C. Piguet, *Chem. Soc. Rev.*, 2005, **34**, 1048; (*b*) M. D. Ward, *Coord. Chem. Rev.*, 2007, **251**, 1663.

4 (*a*) M. Shibasaki and N. Yoshikawa, *Chem. Rev.*, 2002, **102**, 2187; (*b*) O. Guillou, C. Daiguebonne, M. Camara and N. Kerbellec, *Inorg. Chem.*, 2006, **45**, 8468.

5 (*a*) A. Rath, E. Aceves, J. Mitome, J. Liu, U. S. Ozkan and S. G. Shore, *J. Mol. Catal. A: Chem.*, 2001, **165**, 103; (*b*) S. G. Shore, E. Ding, C. Park and M. A. Keane, *Catal. Commun.*, 2002, **3**, 77.

6 (*a*) G. Blasse, *Mater. Chem. Phys.*, 1992, **31**, 3; (*b*) N. Sabatini, M. Guardigli and J. M. Lehn, *Coord. Chem. Rev.*, 1993, **123**, 201; (*c*) Y. Matuura, S. Matsushima, M. Sakamoto and Y. Sadaoka, *J. Mater. Chem.*, 1993, **3**, 767.

7 (*a*) M. L. Kahn, C. Mathonière and O. Kahn, *Inorg. Chem.*, 1999, **38**, 3692; (*b*) Y. C. Liang, R. Cao, W. P. Su, M. C. Hong and W. J. Zhang, *Angew. Chem., Int. Ed.*, 2000, **39**, 3304; (*c*) S. M. Hu, J. C. Dai, X. T. Wu, L. M. Wu, C. P. Cui, Z. Y. Fu, M. C. Hong and Y. C. Liang, *J. Cluster Sci.*, 2002, **13**, 33; (*d*) H. Z. Kou, B. C. Zhou and R. J. Wang, *Inorg. Chem.*, 2003, **42**, 7658; (*e*) J. P. Costes, G. Novitchi, S. Shova, F. Dahan, B. Donnadieu and J. P. Tuchagues, *Inorg. Chem.*, 2004, **43**, 7792; (*f*) S. Ueki, Y. Kobayashi, T. Ishida and T. Nogami, *Chem. Commun.*, 2005, 5223; (*g*) R. Calvo, R. E. Rapp, E. Chagas, R. P. Sartoris, R. Baggio, M. T. Garland and M. Perec, *Inorg. Chem.*, 2008, **47**, 10389.

8 (*a*) O. Guillou, P. Bergerat, O. Kahn, E. Bakalbassis, K. Boubekeur, P. Batail and M. Guillot, *Inorg. Chem.*, 1992, **31**, 110; (*b*) C. Daiguebonne, O. Guillou, M. L. Kahn, O. Kahn, R. L. Oushoorn and K. Boubekeur, *Inorg. Chem.*, 2001, **40**, 176; (*c*) S. M. Liu, E. A. Meyers and S. G. Shore, *Angew. Chem., Int. Ed.*, 2002, **41**, 3609; (*d*) R. Gheorghe, M. Andruh, A. Müller and M. Schmidtmann, *Inorg. Chem.*, 2002, **41**, 5314; (*e*) Q. D. Liu, S. Gao, J. R. Li, B. Q. Ma, Q. Z. Zhou and K. B. Ye, *Polyhedron*, 2002, **21**, 1097; (*f*) J. J. Zhang, S. Q. Xia, T. L. Sheng, S. M. Hu, G. Leibeling, F. Meyer, X. T. Wu, S. C. Xiang and R. B. Fu, *Chem. Commun.*, 2004, 1186; (*g*) H. Z. Kou, Y. B. Jiang and A. L. Cui, *Cryst. Growth & Des.*, 2005, **5**, 77; (*h*) F. He, M. L. Tong, X. L. Yu and X. M. Chen, *Inorg. Chem.*, 2005, **44**, 559; (*i*) A. Q. Wu, G. H. Guo, C. Yang, F. K. Zheng, X. Liu, G. C. Guo, J. S. Huang, Z. C. Dong and Y. Takano, *Eur. J. Inorg. Chem.*, 2005, 1947.

9 *e.g.*: (*a*) J. G. Mao, L. Song, X. Y. Huang and J. S. Huang, *Polyhedron*, 1997, **16**, 963; (*b*) Q. D. Liu, J. R. Li, S. Gao, B. Q. Ma, Q. Z. Zhou, K. B. Ye and H. Liu, *Chem. Commun.*, 2000, 1685; (*c*) Y. P. Ren, L. S. Long, B. W. Mao, Y. Z. Yuan, R. B. Huang and L. S. Zheng, *Angew. Chem., Int. Ed.*, 2003, **44**, 532; (*d*) F. Q. Wang, X. J. Zheng, Y. H. Wan, C. Y. Sun, Z. M. Wang, K. Z. Wang and L. P. Jin, *Inorg. Chem.*, 2007, **46**, 2956; (*e*) J. X. Ma, X. F. Huang, Y. Song, X. Q. Song and W. S. Liu, *Inrog. Chem.*, 2009, **48**, 6326.

10 (*a*) T. Z. Jin, S. F. Zhao, G. X. Xu, Y. Z. Han, N. C. Shi and Z. S. Ma, *Acta Chim. Sin. (Chin. Ed.)*, 1991, **49**, 569; (*b*) T. Yi, G. Gao and B. Li, *Polyhedron*, 1998, **17**, 2243; (*c*) T. K. Prasad, M. V. Rajasekharan and J. P. Costes, *Angew. Chem., Int. Ed.*, 2007, **46**, 2851; (*d*) B. Zhao, P. Cheng, Y. Dai, C. Cheng, D. Z. Liao, S. P. Yan, Z. H. Jiang and G. L. Wang, *Angew. Chem., Int. Ed.*, 2003, **42**, 934; (*e*) B. Zhao, P. Cheng, X. Y. Chen, C. Cheng, W. Shi, D. Z. Liao, S. P. Yan and Z. H. Jiang, *J. Am. Chem. Soc.*, 2004, **126**, 3012; (*f*) B. Zhao, X. Y. Chen, P. Cheng, D. Z. Liao, S. P. Yan and Z. H. Jiang, *J. Am. Chem. Soc.*, 2004, **126**, 15394; (*g*) B. Zhao, H. L. Gao, X. Y. Chen, P. Cheng, W. Shi, D. Z. Liao, S. P. Yan and Z. H. Jiang, *Chem. Eur. J.*, 2006, **12**, 149.

11 (*a*) M. L. Kahn, P. Lecante, M. Verelst, C. Mathonière and O. Kahn, *Chem. Mater.*, 2000, **12**, 3073; (*b*) J. P. Liu, D. W. Knoeppel, S. M. Liu, E. A. Meyers and S. G. Shore, *Inorg. Chem.*, 2001, **40**, 2842; (*c*) Y. Kim, Y. Park and D. Y. Jung, *Dalton Trans.*, 2005, 2603; (*d*) A. Q. Wu, G. H. Guo, F. K. Zheng and M. S. Wang, *Inorg. Chem. Comm.*, 2005, **8**, 1078; (*e*) P. Mahata, K. V. Ramya and S. Natarajan, *Inorg. Chem.*, 2009, **48**, 4942; (*f*) X. Hu, Y. F. Zeng, Z. Chen, E. C. Sañudo, F. C. Liu, J. Ribas and X. H. Bu, *Cryst. Growth & Des.*, 2009, **9**, 421.

12 (*a*) S. Decurtins, M. Gross, H. W. Schmalle and S. Ferlay, *Inorg. Chem.*, 1998, **37**, 2443; (*b*) A. Figuerola, C. Diaz, M. S. El Fallah, J. Ribas, M. Maestro and J. Mahía, *Chem. Commun.*, 2001, 1204; (*c*) B Zhai, L. Yi, H. S. Wang, B. Zhao, P. Cheng, D. Z. Liao and S. P. Yan, *Inorg. Chem.*, 2006, **45**, 8471.

13 (*a*) B. Q. Ma, S. Gao, G. Su and G. X. Xu, *Angew. Chem., Int. Ed.*, 2001, **40**, 434; (*b*) S. Tanase, M. Andruh, A. Mülller, M. Schmidtmann, C. Mathonière and G. Rombaut, *Chem. Commun.*, 2001, 1084; (*c*) S. Gao, G. Su, T. Yi and B. Q. Ma, *Phys. Rev. B*, 2001, **63**, 054431; (*d*) G. M. Li, T. Akitsu, O. Sato and Y. Einaga, *J. Am. Chem. Soc.*, 2003, **125**, 12396; (*e*) T. Akitsu and Y. Einaga, *Polyhedron*, 2006, **25**, 2655; (*f*) W. T. Chen, G. C. Guo, M. S. Wang, G. Xu, L. Z. Cai, T. Akitsu, M. A. Tanaka, A. Matsushita and J. S. Huang, *Inorg. Chem.*, 2007, **46**, 2105.

14 (*a*) J. P. Costes, S. Dupuis and J. P. Laurent, *Eur. J. Inorg. Chem.*, 1998, 1543; (*b*) C. Piguet, E. Rivara-Minten, G. Bernardinelli, J. C. G. Bünzli and G. Hopfgartner, *J. Chem. Soc., Dalton Trans.*, 1997, 421; (*c*) C. Edder, C. Piguet, J. C. G. Bünzli and G. Hopfgartner, *Chem. Eur. J.*, 2001, **7**, 3014; (*d*) J. P. Costes, J. M. Clemente-Juan, F. Dahan, F. Dumestre and J. P. Tuchagues, *Inorg. Chem.*, 2002, **41**, 2886; (*e*) S. Mukherjee, Y. Lan, G. Novitchi, G. E. Kostakis, C. E. Anson and A. K. Powell, *Polyhedron*, 2009, **28**, 1782.

15 (*a*) T. Shiga, H. Ōkawa, S. Kitagawa and M. Ohba, *J. Am. Chem. Soc.*, 2006, **128**, 16426; (*b*) T. Pretsch, K. W. Chapman, G. J. Halder and C. J. Kepert, *Chem. Commun.*, 2006, 1857; (*c*) A. Figuerola, J. Ribas, X. Solans, M. Font-Bardía, M. Maestro and C. Diaz, *Eur. J. Inorg. Chem.*, 2006, 1846; (*d*) A. Figuerola, J. Ribas, M. Llunell, D. Casanova, M. Maestro, S. Alvarea and C. Diaz, *Inorg. Chem.*, 2005, **44**, 6939; (*e*) B. Q. Ma, H. L. Sun and S. Gao, *Chem. Commun.*, 2005, 2336.

16 (*a*) D. M. L. Goodgame, D. A. Grachvogel, A. J. P. White and D. J. Williams, *Inorg. Chem.*, 2001, **40**, 6180; (*b*) P. Mahata, G. Sankar, G. Madras and S. Natarajan, *Chem. Commun.*, 2005, 5787; (*c*) Q. Yue, J. Yang, G. H. Li, G. D. Li, W. Xu, J. S. Chen and S. N. Wang, *Inorg. Chem.*, 2005, **44**, 5241; (*d*) Y. Wang, P. Cheng, J. Chen, D. Z. Liao and S. P. Yan, *Inorg. Chem.*, 2007, **46**, 4530; (*e*) Y. G. Huang, X. T. Wang, F. L. Jiang, S. Gao, M. Y. Wu, Q. Gao, W. Wei and M. C. Hong, *Chem. Eur. J.*, 2008, **14**, 10340.

17 (*a*) M. C. Yin, X. F. Lei, M. Li, L. J. Yuan and J. T. Sun, *J. Phy. Chem. Solids*, 2006, **67**, 1372; (*b*) S. S. Zhao, X. Q. Lü, A. X. Hou, W. Y. Wong, W. K. Wong, X. P. Yang and R. A. Jones, *Dalton Trans.*, 2009, 9595; (*c*) H. L. Gao, B. Zhao, X. Q. Zhao, Y. Song, P. Cheng, D. Z. Liao and S. P. Yan, *Inorg. Chem.*, 2008, **47**, 11057.

18 (*a*) D. M. L. Goodgame, T. E. Müller and D. J. Williams, *Polyhedron*, 1992, **11**, 1513; (*b*) C. Bruoca-Cabarrecq, O. Fava and A. Mosset,

J. Chem. Cryst., 1999, **29**, 81; (*c*) L. Carlucci, G. Ciani, F. Porta, D. M. Proserpio and L. Santagostini, *Angew. Chem., Int. Ed.*, 2002, **41**, 1907; (*d*) T. A. Miller, J. C. Jeffery, M. D. Ward, H. Adams, S. J. A. Pope and S. Faulkner, *Dalton Trans.*, 2004, 1524; (*e*) X. J. Gu and D. F. Xue, *Inorg. Chem.*, 2006, **45**, 9257; (*f*) Y. Q. Sun, J. Zhang and G. Y. Yang, *Chem. Commun.*, 2006, 4700; (*g*) W. F. Yeung, T. C. Lau, X. Y. Wang, S. Gao, L. Szeto and W. T. Wong, *Inorg. Chem.*, 2006, **45**, 6756; (*h*) X. Q. Zhao, B. Zhao, W. Shi and P. Cheng, *CrystEngComm.*, 2009, **11**, 1261; (*i*) X. Q. Zhao, B. Zhao, W. Shi and P. Cheng, *Inorg. Chem.*, 2009, **48**, 11048.

19 (*a*) W. T. Chen, S. M. Ying, D. S. Liu, Q. Y. Luo and Y. P. Xu, *Inorg. Chem. Acta*, 2009, **362**, 2379; (*b*) H. B. Xu, L. Y. Zhang, J. Ni, H. Y. Chao and Z. N. Chen, *Inorg. Chem.*, 2008, **47**, 10744; (*c*) S. G. Baca, S. J. A. Pope, H. Adams and M. D. Ward, *Inorg. Chem.*, 2008, **47**, 3736.

20 (*a*) P. Gütlich, A. Hauser and H. Spiering, *Angew. Chem., Int. Ed. Engl.*, 1994, **33**, 2024; (*b*) H. Toftlund, *Coord. Chem. Rev.*, 1989, **94**, 67.

21 C. E. Plečnik, S. Liu and S. G. Shore, *Acc. Chem. Res.*, 2003, **36**, 499.

22 C. James and P. S. Willand, *J. Am. Chem. Soc.*, 1916, **38**, 1497.

23 *e.g.*: A. E. Crease and P. Legzdins, *J. Chem. Soc., Dalton Trans.*, 1973, 1501.

24 *e.g.*: (*a*) R. Baggio, M. T. Garland, Y. Moreno, O. Peña, M. Perec and E. Spodine, *J. Chem. Soc., Dalton Trans.*, 2000, 2061; (*b*) Y. C. Liang, M. C. Hong, W. P. Su, R. Cao and W. J. Zhang, *Inorg. Chem.*, 2001, **40**, 4574; (*c*) J. P. Costes, G. Novitchi, S. Shova, F. Dahan, B. Donnadieu and J. P. Tuchagues, *Inorg. Chem.*, 2004, **43**, 7792; (*d*) S. C. Xiang, S. M. Hu, T. L. Sheng, J. S. Chen and X. T. Wu, *Chem. Eur. J.*, 2009, **15**, 12496.

25 Y. G. Huang, F. L. Jiang and M. C. Hong, *Coord. Chem. Rev.*, 2009, **253**, 2814.

26 (*a*) Y. C. Liang, R. Cao, W. P. Su and M. C. Hong, *Chem. Lett.*, 2000, 868; (*b*) Y. C. Liang, R. Cao, H. M. Chun, D. F. Sun, Y. J. Zhao, J. B. Weng and R. H. Wang, *Inorg. Chem. Comm.*, 2002, **5**, 366.

27 (*a*) M. B. Zhang, J. Zhang, S. T. Zheng and G. Y. Yang, *Angew. Chem., Int. Ed.*, 2005, **44**, 1385; (*b*) J. W. Cheng, J. Zhang, S. T. Zheng, M. B. Zhang and G. Y. Yang, *Angew. Chem., Int. Ed.*, 2006, **45**, 73; (*c*) J. W. Cheng, S. T. Zheng and G. Y. Yang, *Inorg. Chem.*, 2008, **47**, 4930; (*d*) J. W. Cheng, J. Zhang, S. T. Zheng and G. Y. Yang, *Chem. Eur. J.*, 2008, **14**, 88.

28 (*a*) B. Zhao, X. Y. Chen, Z. Chen, W. Shi, P. Cheng, S. P. Yan and D. Z. Liao, *Chem. Commun.*, 2009, 3113; (*b*) X. Q. Zhao, B. Zhao, Y. Ma, W. Shi, P. Cheng, Z. H. Jiang, D. Z. Liao and S. P. Yan, *Inorg. Chem.*, 2007, **46**, 5832.

29 (*a*) G. M. Sheldrick, *SHELXL-97, Program for the Solution of Crystal Structures*, University of Göttingen (Germany), 1997; (*b*) G. M. Sheldrick, *SHELXL-97, Program for the Refinement of Crystal Structures*, University of Göttingen (Germany), 1997.

30 e.g.: (*a*) R. J. Doedens, E. Yohannes and M. I. Khan, *Chem. Commun.*, 2002, 62; (*b*) S. Noro, R. Kitaura, M. Kondo, S. Kitagawa, T. Ishii, H. Matsuzaka and M. Yamashita, *J. Am. Chem. Soc.*, 2002, **124**, 2568; (*c*) R. Custelcean, C. Afloroaei, M. Vlassa and M. Polverejan, *Angew. Chem., Int. Ed.*, 2000, **39**, 3094; (*d*) N. H. Hu, Z. G. Li, J. W. Xu, H. Q. Jia and J. J. Niu, *Cryst. Growth & Des.*, 2007, **7**, 15.

31 R. Ludwig, *Angew. Chem., Int. Ed.*, 2001, **40**, 1808 and refs therein.

32 (*a*) G. C. Allen and K. R. Hallam, *Appl. Surf. Sci.*, 1996, **93**, 25; (*b*) Wandelt, *Surf. Sci. Reports*, 1982, **2**, 1; (*c*) S. Bera, A. A. M. Prince, S. Velmurugan, P. S. Raghavan, R. Gopalan, G. Panneerselvam and S. V. Narasimhan, *J. Mater. Sci.*, 2001, **36**, 5379.

33 J. A. Real, E. Andres, M. C. Munoz, M. Iulve, T. Granier, A. Bousseksou and F. Varret, *Science*, 1995, **268**, 265.

34 S. Petoud, S. M. Cohen, J. C. G. Bünzli and K. N. Raymond, *J. Am. Chem. Soc.*, 2003, **125**, 13324.

35 C. Tedeschi, J. Azema, H. Gornitzka, P. Tisnes and C. Picard, *Dalton Trans.*, 2003, 1738.

36 G. Vicentini, L. B. Zinner, J. Zukerman-Schpector and K. Zinner, *Coord. Chem. Rev.*, 2000, **196**, 353.

37 Q. H. Xu, L. S. Li, X. S. Liu and R. R. Xu, *Chem. Mater.*, 2002, **14**, 549.

38 N. Arnaud, E. Vaquer and J. Georges, *Analyst.*, 1998, **123**, 261.

39 *e.g.* (*a*) T. Gunnlaugsson, J. P. Leonard, K. Sénéchal and A. J. Harte, *Chem. Commun.*, 2004, 782; (*b*) A. M. Nonat, A. J. Harte, K. Sénéchal-David, J. P. Leonard and T. Gunnlaugsson, *Dalton Trans.*, 2009, 4703.

40 J. C. G. Bunzli and G. R. Chopin, *Lanthanide probes in Life, Chemical and Earth Sciences*, Elsevier, Amsterdam, 1989.

41 (*a*) C. Benelli and D. Gatteschi, *Chem. Rev.*, 2002, **102**, 236; (*b*) H. Sakiyama, R. Ito, H. Kumagai, K. Inoue, M. Sakamoto, Y. Nishida and M. Yamasaki, *Eur. J. Inorg. Chem.*, 2001, 2027; (*c*) F. Klöwer, Y. Lan, J. Nehrkorn, O. Waldmann, C. E. Anson and A. K. Powell, *Chem. Eur. J.*, 2009, **15**, 7413; (*d*) K. C. Mondal, G. E. Kostakis, Y. Lan, C. E. Anson and A. K. Powell, *Inorg. Chem.*, 2009, **48**, 9205.